Mu Opioid Receptor–Positive Neurons in the Dorsal Raphe Nucleus Are Impaired by Morphine Abstinence

Lola Welsch, Esther Colantonio, Camille Falconnier, Cédric Champagnol-Diliberti, Florence Allain, Sami Ben Hamida, Emmanuel Darcq, Pierre-Eric Lutz, Brigitte Kieffer

Mu opioid receptor-positive neurons in the dorsal raphe nucleus are impaired by morphine abstinence

Lola Welsch[1,2], Esther Colantonio[2], Camille Falconnier[3], Florence Allain[1,2], Sami Ben Hamida[1,4], Emmanuel Darcq[1,2], Pierre-Eric Lutz[1,3] and Brigitte L. Kieffer[1,2]

1. Douglas Research Center, Department of Psychiatry, McGill University, Montréal, Quebec H4H 1R3, Canada

2. INSERM U1114, University of Strasbourg, Strasbourg 67084, France

3. Centre National de la Recherche Scientifique, Université de Strasbourg, Institut des Neurosciences Cellulaires et Intégratives UPR3212, 67000 Strasbourg, France

4. INSERM UMR 1247- Research Group on Alcohol & Pharmacodependences (GRAP), Université de Picardie Jules Verne, Amiens, France

Corresponding author:

Brigitte L. Kieffer, INSERM U1114 University of Strasbourg, CRBS 1 rue Eugène Boeckel, CS60026 67084 Strasbourg Cedex France

brigitte.kieffer@unistra.fr

Short title (55 characters): Effects of morphine abstinence on DRN-MOR neurons

Keywords: chronic morphine, mu opioid signaling, addiction-related behaviors, opto-intracranial self-stimulation, vTRAP-seq

ABSTRACT

BACKGROUND. Chronic opioid exposure leads to hedonic deficits and enhanced vulnerability to addiction, which are observed and even strengthen after a period of abstinence, but the underlying circuit mechanisms are poorly understood. In this study, we test the hypothesis that neurons expressing mu opioid receptors (MORs) in the dorsal raphe nucleus (DRN) are involved in addiction vulnerability associated with morphine abstinence, using both molecular and behavioral approaches.

METHODS. MOR-Cre mice were exposed to chronic morphine then went through spontaneous withdrawal for 4 weeks, a well-established mouse model of morphine abstinence. We used viral translating ribosome affinity to profile the transcriptome of DRN-MOR neurons from ABS mice. We also used an opto-intracranial self-stimulation (oICSS) paradigm applied to DRN-MOR neurons, in order to measure responses related to addiction vulnerability: persistence to respond, motivation to obtain the stimulation, self-stimulation despite punishment and cue-induced reinstatement.

RESULTS. Gene expression analyses revealed that DRN-MOR neurons show a down-regulation of genes involved in neuronal excitability and MOR-mediated signaling, including notably the Opioid Reactome. Opto-ICSS data showed that abstinent animals execute more impulsive-like and persistent responses during acquisition, and score higher for addiction-like criteria.

CONCLUSION. Our data suggest that protracted abstinence to chronic morphine leads to reduced MOR function in DRN-MOR neurons, and abnormal self-stimulation of these neurons. We propose that DRN-MOR neurons have partially lost their reward-facilitating properties, which in turn may lead to increased propensity to perform addiction-related behaviors.

INTRODUCTION

Opioid use disorder (OUD) is a chronic brain disorder, characterized by intoxication episodes that are followed by phases of withdrawal, craving and relapse [1]. Acute opioid withdrawal occurs when the drug clears out of the body and is associated with strong physical and psychological symptoms [2], and contribute to the next intoxication episode [3]. Further, after physical withdrawal signs have vanished and abstinence is maintained, hedonic deficits [4-8] develop in the long term, and enhance the risk of relapse [9, 10]. Because maintaining abstinence is a true challenge, the neurobiology of this particular condition is being increasingly studied in preclinical research [11].

The dorsal raphe nucleus (DRN), the main source of serotonin (5-HT) in the central nervous system [12], plays a pivotal role in hedonic tone and mood-related psychiatric disorders or substance abuse [13-15]. There is strong evidence for interactions between opioid and 5-HT systems in the DRN. For example, systemic morphine [16] and heroin [17] increased 5-HT neuron activity in rodents. Rats pretreated with fluoxetine showed enhanced preference for a morphine-associated environment [18] and DRN dopaminergic neurons were necessary for the expression of morphine conditioned place preference [19]. In addition, opioid withdrawal is associated with impaired DRN activity. For example, opioid-dependent rats showed lower 5-HT release in response to morphine compared to naïve controls [20], naltrexone-precipitated withdrawal decreased DRN 5-HT levels [20], and 5-HT2C receptor activation suppressed physical withdrawal symptoms upon naloxone-precipitated withdrawal [21]. Also, adaptations in glutamatergic inputs from the lateral habenula to the DRN were shown involved in social deficits associated with naloxone-precipitated withdrawal [22], and expression levels of BDNF, TrkB and CRF-R1 mRNAs were decreased in 5-HT neurons of the DRN during both morphine exposure and after seven days of withdrawal [23]. Although non-exhaustive, this set of studies clearly demonstrates implication of the DRN and 5HT transmission in opioid dependence.

We previously developed a mouse model of protracted abstinence to chronic morphine, which revealed the emergence of social interaction deficits and despair-like behavior four

weeks after cessation of the chronic morphine exposure [24]. Conditional deletion of MORs in the DRN prior to morphine exposure [25] and fluoxetine treatment during abstinence [24, 26] prevented the emergence of these phenotypes in abstinent animals, demonstrating a causal link between chronic receptor activation in the DRN and emotional responses. Here, we used the same mouse model of morphine abstinence to study neurons expressing the receptor (DRN-MOR neurons), as these neurons represent the primary cellular target of opioids in the DRN. We tested the hypothesis that DRN-MOR neurons have adapted to morphine with both molecular and behavioral consequences related to addiction. We found significant downregulation of the Opioid Reactome in DRN-MOR neurons of abstinent animals, and also discovered higher propensity of these animals to opto-self-stimulate these neurons.

METHODS AND MATERIALS

See **Suppl Information** for detailed Methods and Materials

Animals

Adult male mice (20-40g) used for experiments were group housed in a temperature- and humidity- controlled animal facility (21±4°C, 45± 10% humidity) on a 12h dark/light cycle. MOR-Cre knock-in mice [27] were given access to food and water *ad libitum*, unless otherwise noted. All mice were monitored for health status daily during experimentation for the entirety of the study. All experiments were performed in accordance with the Canadian Council of animal Care and by the Animal Care Committees.

Morphine treatment

Morphine sulfate (NIH, NIDA Drug Supply Program) was prepared in saline (0.98% sodium chloride) and injected twice daily intraperitoneally with escalating doses of morphine (20, 40, 60, 80, 100 mg/kg for 5 days, followed by a single 100mg/kg injection on day 6), according to our previously described protocol [24, 28]

RNA sequencing

MOR-Cre male mice were injected with 500nL of AAV2-hSyn-DIO-L10a-mCherry in the DRN. Three weeks after virus injection, mice were injected with chronic morphine and after four weeks of abstinence, DRN of these mice were collected and we proceeded to mRNA extraction of whole tissue (input) and ribosome-bound immuno-precipitated (IP) mRNAs. For RNA-sequencing analysis, we used principal component analysis (PCA), over-representation analysis and gene set enrichment analysis.

Operant optogenetic self-stimulation

MOR-Cre male mice were injected with 500nL of AAV2-hsyn-DIO-ChR2-mCherry in the DRN and implanted with an optic fiber above the DRN. Three weeks after virus injection, mice were subjected to the chronic morphine treatment, then behaviorally tested 4 weeks later (see **Suppl Information** for details).

RESULTS

Enrichment of DRN-MOR neurons for gene expression analysis

We first examined whether the prior history of chronic morphine exposure durably modifies gene expression in DRN-MOR neurons. To specifically analyze gene expression in these neurons, we used viral translating ribosome affinity purification (vTRAP) methodology [29]. We targeted expression of a L10a-mCherry ribosomal transgene to these neurons by injection of a Cre-dependent virus in the DRN of MOR-Cre mice (**Figure 1A**). Animals were subsequently exposed to chronic morphine or saline. Four weeks later, the DRN was micro-dissected and we proceeded to the separation of RNA fractions coming from total DRN tissue (input) or from immuno-precipitated (IP) ribosomes. The two RNA fractions were used for RNA-Seq library preparation and sequenced at similar depth (**Suppl Figure S1**; two-way ANOVA, Fraction effect, n.s.) with no difference between treatments (two-way ANOVA, Treatment effect, n.s.).

A PCA analysis performed on all samples (IP and input) from control (CTL) and abstinent (ABS) animals revealed that factor 1, explaining 41.71% of the total variance, discriminated IP from input samples (**Figure 1B**; two-way RM ANOVA, Fraction effect, $p<0.0001$). In addition, as expected, IP versus input samples showed higher expression counts for MOR (**Figure 1C**; two-way RM ANOVA, Fraction effect, $p<0.01$) and mCherry (**Figure 1D**; two-way RM ANOVA, Fraction effect, $p<0.05$), suggesting that the procedure successfully enriched MOR-neurons in the IP fraction. This enrichment was similar for CTL and ABS groups (**Figure 1C-D**; two-way RM ANOVA, Treatment effect, n.s.), enabling unbiased assessment of abstinence-related differences.

We also compared differentially expressed genes in IP vs input samples of CTL mice with recent single-cell expression data generated in the DRN [30] (**Suppl Figure S2**). We found that IP samples were depleted in markers genes for several non-neuronal cell types (oligodendrocytes, polydendrocytes), and enriched for markers of one type of serotonergic neurons, two types of GABAergic neurons and three types of glutamatergic neurons, which matches our own immunohistochemical characterization indicating that DRN-MOR neurons are mainly glutamatergic and GABAergic, and for a smaller proportion serotonergic (unpublished). Altogether, these results show that the vTRAP procedure enables the analysis of morphine abstinence effects in an enriched DRN-MOR neuron population.

The transcriptome of DRN-MOR neurons is modified in abstinent mice

We next analyzed whether gene expression is modified in ABS animals by comparing input or IP RNA-seq data from ABS and CTL mice. While a similar number of genes were differentially expressed at nominal significance ($p<0.05$) in IP (613 genes) and input RNA fractions (617 genes), there was little overlap between the two (Jaccard index ±3%, 36 differentially expressed genes in common, **Figure 2A**). Further, morphine abstinence was associated with down-regulation of gene expression (**Figure 2B**) in both IP (406/613 downregulated genes; One sample t-test, $p<0.0001$) and input fractions (340/617 downregulated genes; one sample t-test, $p<0.01$). This pattern of downregulation was more pronounced in the IP vs input (**Figure**

2B, unpaired t-test, p<0.0001), suggesting that the global transcriptional impact of abstinence is different and stronger in DRN-MOR neurons. This was confirmed by the observation that, compared to the whole genome, genes that were differentially expressed as a function of abstinence in the IP (**Figure 2C**) showed significantly higher fold changes in the IP/input comparison (unpaired t-test, p<0.0001).

We then conducted a gene ontology analysis [31] (**Figure 2D and Suppl Tables S1-5**) of differentially expressed genes in DRN-MOR neurons. The top 10 gene ontology terms that were significantly over-represented in ABS vs CTL IP samples related to the regulation of neuronal excitability and ion conductance (**Suppl Tables S1-2**). Notably genes regulating potassium (K^+) efflux from neuronal cells were downregulated including *Kcnj14*, *Kcnk6*, *Kcnn4*, *Kcnmb4* and *Kcns2*, or genes associated with sodium exchanges (*Scn4b*), and voltage–dependent regulation of calcium (Ca^{2+}) influx (*Cacng3, Cacng5, Cacna1d).* Genes such as *Gabra3* (GABA A receptor, subunit alpha 3) or *Htr3a* (5-HT receptor 3A) were also decreased (**Suppl Table S1**) suggesting that morphine abstinence alters neurotransmission in DRN-MOR neurons. Other sets of differentially expressed genes were linked to axon formation including genes for microtubules functions (*Dnah9, Dnah5, Dnah10, Dnah7a* or *Kif3b),* and ciliary functions (*Cfap206, Cfap52, Cep162)* (**Suppl Table S3**), indicative of cellular morphology changes.

We next used gene set enrichment analysis [32] to further characterize the impact of morphine abstinence on the Opioid Reactome [33], an annotated gene list that is composed of genes known to be involved in opioid signaling (±90 genes, see **Suppl Table S6**), including *Oprm1* itself, classical intracellular messengers of GPCR-regulated pathways (such as G protein subunits and adenylate cyclases) and proteins involved in downstream phosphorylation cascades (e.g. calcium/calmodulin kinases or protein kinase C alpha and gamma). We found enrichment of the Opioid Reactome in IP fractions compared to input for CTL and ABS samples (**Figure 2E**, FDR BH, CTL: q=0.18; ABS: q=0.35), a trend that did not reach significance but still consistent with the enrichment of DRN-MOR neurons in IP samples (**Figure 2E**). Interestingly, comparison of CTL and ABS IP fractions revealed a significant depletion of the

Opioid Reactome in DRN-MOR neurons of ABS mice (**Figure 2F**, FDR BH, q<0.05), suggesting that morphine abstinence reduces expression levels of genes involved in MOR activity and the associated intracellular signaling pathways.

Together RNA-seq data demonstrate that DRN-MOR neurons of ABS animals show a specific down-regulation of genes related to neuronal excitability and MOR signaling, which possibly alters their function.

An oICSS paradigm to study reward-related behaviors controlled by DRN-MOR neurons

Our prior experiments had shown that mice self-administer the opto-stimulation of their DRN-MOR neurons (unpublished), demonstrating that activation of these neurons has rewarding properties, and consistent with previous work [34]. We therefore tested whether this behavior, referred as to opto-intracranial self-stimulation (oICSS), is modified in ABS animals.

MOR-Cre mice were injected in the DRN with a Cre-inducible virus expressing ChR2 fused to mCherry (**Suppl Fig S3)**, or mCherry alone, and implanted with an optic fiber targeting the DRN (**Figure 3A**). Three weeks after surgeries, mice were submitted to the chronic saline (CTL) or morphine (ABS) treatment, and the acquisition of self-stimulation started 28 days after the last morphine injection [24, 25]. Animals were trained to self-administer the laser stimulation (LS) during 28 consecutive days under a fixed ratio (FR) that gradually increased from FR1 to FR5. The operant paradigm was also designed as to measure the persistence to respond during time-off periods. Next, we tested i) the motivation to obtain the LS in a progressive ratio procedure, ii) the level of compulsive-like behaviors, evaluated as nosepoking despite receiving a foot-shock, iii) reinstatement of the oICSS behavior, measured as cue-induced nosepoking after extinction training.

Control and abstinent mice self-stimulate their DRN-MOR neurons

CTL mice discriminated between the active and inactive nosepoke (**Figure 1B,** left; three-way RM ANOVA, NP effect, p<0.0001) and the number of active responses increased from FR1 (66 ± 9 active nosepokes/session) to FR3 (148 ± 11 active nosepokes/session) and FR5

schedules (196 ± 12 active nosepokes/session) (three-way RM ANOVA, Schedule effect, $p<0.0001$). ABS animals seemed to self-stimulate at higher levels (FR1: 84 ± 10 active nosepokes/session; FR3: 176 ± 14 active nosepokes/session; FR5: 228 ± 18 active nosepokes/session) during the entire oICSS experiment, but the statistical analysis showed no significant difference between the CTL and ABS groups (**Figure 1B,** right; three-way RM ANOVA, Treatment effect, n.s.).

The number of LS earned during each 1-hour operant session remained stable across schedules for the two groups (**Figure 1C**; two-way ANOVA, Schedule effect, n.s.): both CTL and ABS mice adapted their nosepokes to receive 41 ± 1 LS/session (38 ± 1 and 43 ± 1 LS respectively) across the acquisition period. As expected, none of the mCherry-mice achieved the acquisition criteria (**Suppl Figure S4A**), demonstrating that the self-stimulation behavior was specific to DRN-MOR neuron activation. A post-mortem analysis confirmed that the LS induced a significant increase in the number of c-Fos+ cells in the DRN of ChR2-mice compared to mCherry-mice (**Suppl Figure S4B-C**; Kruskal-Wallis test, virus effect, $p<0.01$), and for both CTL ($p<0.01$) and ABS ($p<0.01$) groups. The data confirm our prior study showing that DRN-MOR neuron opto-activation has reinforcing properties, and also suggest that acquisition of this behavior does not differ in ABS mice.

Abstinent mice perform more impulsivity-like nose pokes and persistent responses during the acquisition of oICSS

Although ABS mice did not differ from CTL mice in the number of nosepoke and LS earned per session, other parameters indicate differences between the two groups. ABS mice performed on average more impulse-like nosepokes (performed during the first 5 sec of the session with cue-light on and LS off, see [35] and **Suppl Figure S5A**) than CTL mice (**Figure 4A;** three-way RM ANOVA, Treatment effect, $p<0.05$). Nosepokes performed during the following 15s (Two-way RM ANOVA, Treatment effect, $p=0.1501$, **Suppl Figure S5B**) was similar in the two groups, further supporting the notion of impulsive-like responses [35, 36]. Locomotor activity across all sessions (Two-way RM ANOVA, Treatment effect, $p=0.42$, **Suppl**

Figure S5C) also was similar, suggesting that no general hyperactivity interferes with these responses.

We also measured the persistence to respond by introducing a time-off period (no light cue, no LS), in the middle of the oICSS session during FR3 and FR5 sessions [37, 38]. ABS mice performed more active responses during the time-off period in the FR3 schedule (40 ± 3) compared to CTL mice (29 ± 2; **Figure 4B**; three-way RM ANOVA, effect of Treatment, $p<0.05$). This result indicates that ABS animals show a more limited ability to inhibit a response once it is initiated.

Abstinent mice display more addiction-related criteria than control mice

Next we recorded motivation to obtain the LS, compulsivity-like behavior and cue-induced reinstatement of the oICSS behavior. During the progressive ratio session, CTL mice performed 396 ± 36 active nosepokes while ABS mice performed 433 ± 38 active nosepokes in total (**Figure 4C**; unpaired t-test, n.s.). During the foot-shock session, CTL mice earned 11 ± 1 LS in total, while ABS mice earned 13 ± 1 LS (**Figure 4D**; unpaired t-test, n.s.). After the foot-shock session, mice were trained under a FR5 schedule to restore baseline nosepoking and earned LS (**Suppl Figure S6A-B)**, and the self-stimulation behavior was subsequently extinguished during 10 days. No physical withdrawal sign was observed during extinction.

During the last extinction session, CTL and ABS mice performed 15 ± 2 and 21 ± 3 active nosepokes, respectively (**Figure 4E**; two-way RM ANOVA, Treatment effect, n.s.). During the cue-induced reinstatement session, both CTL and ABS mice re-established nosepoking (**Figure 4E**; two-way RM ANOVA, Cue effect, $p<0.01$) and performed similarly with 28 ± 4 and 34 ± 7 active nosepokes, respectively (**Figure 4E**; two-way RM ANOVA, Treatment effect, n.s.). None of the group comparison revealed a significant effect of morphine abstinence, suggesting that motivation, compulsive-like behavior and reinstatement were similar for CTL and ABS mice.

Yet ABS mice tended to score slightly higher than CTL for each measured behavior, which prompted us to perform a three-criteria analysis that takes advantage of inter-individual

variability [37, 39] (**Figure 5**). This analysis separates mice into four groups ranging from 0 to 3 criteria of addiction-related behaviors [37]. As previously done for cocaine [37] and sucrose self-administration [39], we correlated intensity of responses in the three tests with the intensity of the criterion met by each mouse: mice with the higher criteria of addiction-related behaviors were also mice that scored higher for persistence to respond (**Figure 5A**; Kruskal-Wallis test, Criteria effect, $p<0.001$), motivation (**Figure 5B**; Kruskal-Wallis test, Criteria effect, $p<0.01$) and compulsivity-like behavior (**Figure 5C**; Kruskal-Wallis test, Criteria effect, $p<0.05$).

The four groups were distributed differently among CTL and ABS animals (**Figure 5D**), so that 52.9% CTL mice presented 0 criteria vs 11.8% for ABS mice, and only 5.9% CTL mice reached 3 criteria vs 17.6% for ABS mice. In addition, ABS mice were in average attributed more addiction-related criteria that CTL mice (**Figure 5E**; Chi-square test for trend, $p<0.05$). This analysis demonstrates that morphine abstinence induces a shift towards a higher score in the three-criteria analysis.

We finally performed a PCA analysis with data collected for persistence, motivation, compulsion and reinstatement tests (**Figure 5F**: variables' space, **Figure 5G-H**: subjects' space). The first factor aggregated the four behavioral tests and explained 45.3% of the variance. Projection in the subjects' space revealed that Factor 1 clustered individuals according to their addiction-related criteria (**Figure 5G**, one-way RM ANOVA on Factor 1, $p<0.0001$), and subjects were ranked according to their number of criteria along the Factor 1 axis: the higher the values in Factor 1, the higher the criteria of addiction-related behaviors, suggesting that Factor 1 reflects the expression of addiction-related behaviors. In addition, Factor 1 also significantly dissociated CTL from ABS mice (**Figure 5H**; unpaired t-test, $p<0.05$), demonstrating distinct patterns of addiction-related behaviors across the two populations. In line with the three-criteria analysis, this result shows that an individual-based analysis allows a significant separation of ABS and CTL animals, and suggests that the prior exposure to morphine enhances the propensity to perform addiction-related behaviors in the DRN-MOR neuron oICSS paradigm.

DISCUSSION

In summary, our data show an alteration of DRN-MOR neuron function in morphine ABS animals at both molecular and behavioral levels. At present, only few neuronal types or microcircuits have been show modified upon protracted abstinence to morphine, and these include kappa opioid receptor-expressing neurons in the DRN projecting to the NAc [40], the VTA-tVTA circuit [41] or the amygdala-NAC pathway [42]. Here we show for the first-time major alterations in cells that are the primary target of morphine within a major mood center.

Morphine abstinence impairs the transcriptome of DRN-MOR neurons

Our laboratory reported transcriptional modifications developing during morphine abstinence, notably in the extended amygdala [28, 43], however a cell-specific characterization of morphine abstinence effects has not been done. Using vTRAP in MOR-Cre mice, we were able to isolate and sequence the transcriptome of DRN-MOR neurons.

Differentially expressed genes (CTL vs ABS) largely differed in total DRN tissue versus enriched DRN-MOR neurons. This observation is in line with the significant enrichment of DRN-MOR neurons in IP samples, which results from the high Cre/MOR co-localization demonstrated in MOR-Cre mice [27]. Also, the effect size of abstinence was higher in DRN-MOR neurons, suggesting that the chronic morphine regimen has a higher impact on the transcriptome of MOR-neurons compared to whole DRN tissue. This finding is consistent with the notion that MOR-neurons are the primary pharmacological target of opioids in the brain, and encourages future experiments using vTRAP in MOR-Cre mice to better grasp subtle transcriptional modifications in opioid studies across the brain.

The gene ontology analysis shows major alterations in the expression of ion channel-encoding genes, suggesting that protracted morphine abstinence modifies ion conductance in DRN-MOR neurons. Notably, the expression of genes associated with K^+ efflux and voltage–dependent regulation of Ca^{2+} influx in neuronal cells were modified in ABS animals, which

could modify the intrinsic excitability of DRN-MOR neurons and disrupt neurotransmitter release [44-46]. Therefore, both neuronal function and opioid sensitivity of DRN-MOR neurons are likely impaired by a prior history of morphine exposure.

The gene set enrichment analysis also demonstrates a downregulation of the Opioid Reactome in DRN-MOR neurons of ABS individuals. This is consistent with previous studies revealing modifications in several major GPCR signaling pathways [28, 47, 48] and reduced *Penk* expression upon long-term morphine withdrawal [43]. Even though these results were collected from other brain regions and bulk tissue, these studies together with our data, support the notion that morphine abstinence reduces GPCR signaling, including opioid reactivity, in brain regions associated with the modulation of reward and affective responses.

oICSS of DRN-MOR neurons is a useful approach to study reward seeking behaviors in the context of morphine abstinence

oICSS was used previously to evaluate the reinforcing properties of selected neuronal populations [49-53]. More recently, Pascoli et al. proposed that oICSS of dopaminergic neurons (oDASS) located in the ventral tegmental area can also be used as a model of compulsive drug-taking in mice. The authors demonstrated that oDASS was sufficient to recapitulate some behavioral hallmarks of addiction, including compulsive responding for the LS despite a foot-shock [35]. Our own paradigm was based on this study: mice trained to self-stimulate their DRN-MOR neurons reached 41 LS in 1 hour, while mice trained with oDASS obtained 80 LS in a 45 min [35]. Despite the lower level of self-stimulation for oICSS of DRN-MOR neurons, mice in our study controlled the total number of LS received across sessions just as for oDASS [35], suggesting the existence of a hedonic threshold specific to each reinforcer (drug infusion or opto-stimulation of different neuronal population) [35, 54, 55].

Mice self-stimulating DRN-MOR neurons developed behavioral responses observed in rodent drug self-administration models classically used in rodent addiction research [37, 56-58], including impulsivity-like responses, persistent responses, compulsivity-like responses, and cue-induced reinstatement [59, 60]. Therefore, the DRN-MOR neuron oICSS paradigm

seems to be an appropriate approach to test whether morphine abstinence has consequences on reward seeking and possibly vulnerability to develop addiction-like behaviors. Morphine self-administration could have been used but re-exposition to the drug would hinder neuro-adaptations specific to the ABS state. Sucrose self-administration also would be inappropriate because opioid abstinence was shown to decrease sucrose preference [25, 61, 62] and self-administration [63].

Protracted morphine abstinence increases vulnerability to perform addiction-related behaviors

Nosepokes and earned LS were similar for ABS and CTL mice during acquisition, suggesting that reinforcing properties of the ChR2-mediated activation of DRN-MOR neurons are intact in ABS mice, despite altered expression of genes related to neuronal excitability and opioid signaling. However, other oICSS responses were different: first, ABS mice performed more non-rewarded active nosepokes between at the onset of the cue-light (first 5s), considered a marker of impulsivity predictive of future vulnerability to addiction [35, 64-68] and consistent with the human literature showing persistent impulsivity in former heroin users [69-72]. Second, ABS mice are more prone to perform addiction-related behaviors in the three-criteria analysis. This result is coherent with pre-clinical studies showing that prior opioid exposure increased opioid self-administration [73-75] and clinical work designating prior opioid exposure as a major risk factor for addiction to opioids [76-80] and other drugs [81]. This also strengthens the idea that chronic opioids induce neuroadaptations that will later drive addiction [10]. An important next step would be to investigate whether this particular behavioral adaptation is detectable through the manipulation of other brain circuits, by testing oICSS of other populations of MOR-neurons. Another important step will be to perform a similar study in female mice, as gender differences are reported in opioid abstinence [73, 82-84].

DRN-mediated mechanisms underlying behavioral alterations in protracted abstinence to chronic morphine: a possible reward deficiency?

The present study demonstrates that a prior history of chronic morphine exposure followed by a period of protracted abstinence leads to (i) a downregulation of gene clusters involved in neuronal excitability and GPCR signaling, including the MOR-regulated pathway, in DRN-MOR neurons and (ii) the emergence of increased impulsivity and higher propensity to perform addiction-related behaviors in the DRN-MOR neuron oICSS paradigm. The behavioral phenotype of ABS animals could be interpreted as a consequence of reduced DRN-MOR function, which may in turn jeopardize reward processing ensured by these neurons, and lead to enhanced reward seeking behavior. In a previous study, we reported increased passive coping behavior and reduced social interactions in ABS animals, using the same chronic morphine paradigm [25], and demonstrated the implication of MORs in the DRN in the emergence of social interaction deficits [25]. It is possible that the observed negative affective state in the latter study also results from altered reward processing by dysfunctional DRN-MOR neurons. Future investigations will establish whether a causal link exists between transcriptional modifications in DRN-MOR neurons, altered neuronal physiology, and maladaptive reward processing.

ACKNOWLEDGMENTS AND DISCLOSURES

This work was supported by the National Institutes of Health (P50DA005010 and R01048796 to BLK), the Canada Fund for Innovation and the Canada Research Chairs (ED and BLK), Support was also received from the 'Centre National de la Recherche Scientifique' (CF and PEL), Strasbourg University (CF and PEL), French National Research Agency (ANR-19-CE37-0010; PEL), 'Fondation Fyssen' ('subvention recherche 2021'; PEL), and 'Fondation pour la Recherche Médicale' (FDT202204015236; CF). Sequencing was performed by the GenomEast platform, a member of the 'France Génomique' consortium (ANR-10-INBS-0009). We also thank the staff of the animal facility of the Neurophenotyping Center of the Douglas Mental Health University Institute (Montréal, Canada).

LW, PEL and BLK designed the experiments. LW, EC, CF performed the experiments. ED, PEL, SBH and FA helped for experimental design and data analysis. BLK and LW wrote the manuscript. BLK provided resources for the study. All authors read and approved the submitted version.

The authors report no biomedical financial interests or potential conflicts of interest

REFERENCES

1. Koob, G.F. and N.D. Volkow, *Neurobiology of addiction: a neurocircuitry analysis.* Lancet Psychiatry, 2016. **3**(8): p. 760-773.
2. Kosten, T.R. and L.E. Baxter, *Review article: Effective management of opioid withdrawal symptoms: A gateway to opioid dependence treatment.* Am J Addict, 2019. **28**(2): p. 55-62.
3. Hutcheson, D.M., et al., *The role of withdrawal in heroin addiction: enhances reward or promotes avoidance?* Nat Neurosci, 2001. **4**(9): p. 943-7.
4. Kenny, P.J., et al., *Conditioned withdrawal drives heroin consumption and decreases reward sensitivity.* J Neurosci, 2006. **26**(22): p. 5894-900.
5. Swain, Y., et al., *Higher anhedonia during withdrawal from initial opioid exposure is protective against subsequent opioid self-administration in rats.* Psychopharmacology (Berl), 2020. **237**(8): p. 2279-2291.
6. Holtz, N.A., et al., *Intracranial self-stimulation reward thresholds during morphine withdrawal in rats bred for high (HiS) and low (LoS) saccharin intake.* Brain Res, 2015. **1602**: p. 119-26.
7. Schaefer, G.J. and R.P. Michael, *Changes in response rates and reinforcement thresholds for intracranial self-stimulation during morphine withdrawal.* Pharmacology Biochemistry and Behavior, 1986. **25**(6): p. 1263-1269.
8. Schaefer, G.J. and R.P. Michael, *Morphine withdrawal produces differential effects on the rate of lever-pressing for brain self-stimulation in the hypothalamus and midbrain in rats.* Pharmacology Biochemistry and Behavior, 1983. **18**(4): p. 571-577.
9. Baker, T.B., et al., *Addiction motivation reformulated: an affective processing model of negative reinforcement.* Psychol Rev, 2004. **111**(1): p. 33-51.
10. Evans, C.J. and C.M. Cahill, *Neurobiology of opioid dependence in creating addiction vulnerability.* F1000Res, 2016. **5**.

11. Welsch, L., et al., *The Negative Affect of Protracted Opioid Abstinence: Progress and Perspectives From Rodent Models.* Biol Psychiatry, 2020. **87**(1): p. 54-63.
12. Jacobs, B.L. and E.C. Azmitia, *Structure and function of the brain serotonin system.* Physiol Rev, 1992. **72**(1): p. 165-229.
13. Baldwin, D. and S. Rudge, *The role of serotonin in depression and anxiety.* Int Clin Psychopharmacol, 1995. **9 Suppl 4**: p. 41-5.
14. Valentino, R.J., I. Lucki, and E. Van Bockstaele, *Corticotropin-releasing factor in the dorsal raphe nucleus: Linking stress coping and addiction.* Brain Res, 2010. **1314**: p. 29-37.
15. Kirby, L.G., F.D. Zeeb, and C.A. Winstanley, *Contributions of serotonin in addiction vulnerability.* Neuropharmacology, 2011. **61**(3): p. 421-32.
16. Tao, R. and S.B. Auerbach, *GABAergic and glutamatergic afferents in the dorsal raphe nucleus mediate morphine-induced increases in serotonin efflux in the rat central nervous system.* J Pharmacol Exp Ther, 2002. **303**(2): p. 704-10.
17. Wei, C., et al., *Response dynamics of midbrain dopamine neurons and serotonin neurons to heroin, nicotine, cocaine, and MDMA.* Cell Discov, 2018. **4**: p. 60.
18. Harris, G.C. and G. Aston-Jones, *Augmented Accumbal Serotonin Levels Decrease the Preference for a Morphine Associated Environment During Withdrawal.* Neuropsychopharmacology, 2001. **24**(1): p. 75-85.
19. Lin, R., et al., *The Raphe Dopamine System Controls the Expression of Incentive Memory.* Neuron, 2020. **106**(3): p. 498-514.e8.
20. Tao, R., Z. Ma, and S.B. Auerbach, *Alteration in regulation of serotonin release in rat dorsal raphe nucleus after prolonged exposure to morphine.* J Pharmacol Exp Ther, 1998. **286**(1): p. 481-8.
21. Zhang, G., et al., *Activation of serotonin 5-HT(2C) receptor suppresses behavioral sensitization and naloxone-precipitated withdrawal symptoms in morphine-dependent mice.* Neuropharmacology, 2016. **101**: p. 246-54.

22. Valentinova, K., et al., *Morphine withdrawal recruits lateral habenula cytokine signaling to reduce synaptic excitation and sociability.* Nature Neuroscience, 2019. **22**(7): p. 1053-1056.

23. Lunden, J.W. and L.G. Kirby, *Opiate exposure and withdrawal dynamically regulate mRNA expression in the serotonergic dorsal raphe nucleus.* Neuroscience, 2013. **254**: p. 160-172.

24. Goeldner, C., et al., *Impaired emotional-like behavior and serotonergic function during protracted abstinence from chronic morphine.* Biological psychiatry, 2011. **69**(3): p. 236-244.

25. Lutz, P.-E., et al., *Distinct mu, delta, and kappa opioid receptor mechanisms underlie low sociability and depressive-like behaviors during heroin abstinence.* Neuropsychopharmacology : official publication of the American College of Neuropsychopharmacology, 2014. **39**(11): p. 2694-2705.

26. Lalanne, L., et al., *Kappa opioid receptor antagonism and chronic antidepressant treatment have beneficial activities on social interactions and grooming deficits during heroin abstinence.* Addict Biol, 2017. **22**(4): p. 1010-1021.

27. Bailly, J., et al., *Targeting Morphine-Responsive Neurons: Generation of a Knock-In Mouse Line Expressing Cre Recombinase from the Mu-Opioid Receptor Gene Locus.* eneuro, 2020. **7**(3): p. ENEURO.0433-19.2020.

28. Le Merrer, J., et al., *Protracted abstinence from distinct drugs of abuse shows regulation of a common gene network.* Addict Biol, 2012. **17**(1): p. 1-12.

29. Nectow, A.R., et al., *Rapid Molecular Profiling of Defined Cell Types Using Viral TRAP.* Cell Rep, 2017. **19**(3): p. 655-667.

30. Huang, K.W., et al., *Molecular and anatomical organization of the dorsal raphe nucleus.* eLife, 2019. **8**: p. e46464.

31. Liao, Y., et al., *WebGestalt 2019: gene set analysis toolkit with revamped UIs and APIs.* Nucleic Acids Res, 2019. **47**(W1): p. W199-w205.

32. Subramanian, A., et al., *Gene set enrichment analysis: A knowledge-based approach for interpreting genome-wide expression profiles.* Proceedings of the National Academy of Sciences, 2005. **102**(43): p. 15545-15550.

33. Jassal, B.L.N., N., *Opioid Signalling.* Reactome, 2004.

34. Castro, D.C., et al., *An endogenous opioid circuit determines state-dependent reward consumption.* Nature, 2021. **598**(7882): p. 646-651.

35. Pascoli, V., et al., *Sufficiency of Mesolimbic Dopamine Neuron Stimulation for the Progression to Addiction.* Neuron, 2015. **88**(5): p. 1054-1066.

36. Mancino, S., et al., *Epigenetic and Proteomic Expression Changes Promoted by Eating Addictive-Like Behavior.* Neuropsychopharmacology, 2015. **40**(12): p. 2788-2800.

37. Deroche-Gamonet, V., D. Belin, and P.V. Piazza, *Evidence for Addiction-like Behavior in the Rat.* Science, 2004. **305**(5686): p. 1014-1017.

38. Logan, G.D., R.J. Schachar, and R. Tannock, *Impulsivity and Inhibitory Control.* Psychological Science, 1997. **8**(1): p. 60-64.

39. Domingo-Rodriguez, L., et al., *A specific prelimbic-nucleus accumbens pathway controls resilience versus vulnerability to food addiction.* Nature Communications, 2020. **11**(1): p. 782.

40. Pomrenze, M.B., et al., *Modulation of 5-HT release by dynorphin mediates social deficits during opioid withdrawal.* Neuron, 2022.

41. Kaufling, J. and G. Aston-Jones, *Persistent Adaptations in Afferents to Ventral Tegmental Dopamine Neurons after Opiate Withdrawal.* J Neurosci, 2015. **35**(28): p. 10290-303.

42. Zan, G.Y., et al., *Amygdalar κ-opioid receptor-dependent upregulating glutamate transporter 1 mediates depressive-like behaviors of opioid abstinence.* Cell Rep, 2021. **37**(5): p. 109913.

43. Becker, J.A.J., B.L. Kieffer, and J. Le Merrer, *Differential behavioral and molecular alterations upon protracted abstinence from cocaine versus morphine, nicotine, THC and alcohol.* Addiction Biology, 2017. **22**(5): p. 1205-1217.

44. Fornasari, D., *Pain pharmacology: focus on opioids.* Clin Cases Miner Bone Metab, 2014. **11**(3): p. 165-8.

45. Cohen, G.A., V.A. Doze, and D.V. Madison, *Opioid inhibition of GABA release from presynaptic terminals of rat hippocampal interneurons.* Neuron, 1992. **9**(2): p. 325-335.

46. Johnson, S.W. and R.A. North, *Opioids excite dopamine neurons by hyperpolarization of local interneurons.* J Neurosci, 1992. **12**(2): p. 483-8.

47. Terwilliger, R.Z., et al., *A general role for adaptations in G-proteins and the cyclic AMP system in mediating the chronic actions of morphine and cocaine on neuronal function.* Brain Res, 1991. **548**(1-2): p. 100-10.

48. Jolas, T., E.J. Nestler, and G.K. Aghajanian, *Chronic morphine increases GABA tone on serotonergic neurons of the dorsal raphe nucleus: association with an up-regulation of the cyclic AMP pathway.* Neuroscience, 2000. **95**(2): p. 433-43.

49. Faget, L., et al., *Opponent control of behavioral reinforcement by inhibitory and excitatory projections from the ventral pallidum.* Nature Communications, 2018. **9**(1): p. 849.

50. Zell, V., et al., *VTA Glutamate Neuron Activity Drives Positive Reinforcement Absent Dopamine Co-release.* Neuron, 2020. **107**(5): p. 864-873.e4.

51. Tooley, J., et al., *Glutamatergic Ventral Pallidal Neurons Modulate Activity of the Habenula-Tegmental Circuitry and Constrain Reward Seeking.* Biol Psychiatry, 2018. **83**(12): p. 1012-1023.

52. Nieh, E.H., et al., *Inhibitory Input from the Lateral Hypothalamus to the Ventral Tegmental Area Disinhibits Dopamine Neurons and Promotes Behavioral Activation.* Neuron, 2016. **90**(6): p. 1286-1298.

53. Urstadt, K.R. and K.C. Berridge, *Optogenetic mapping of feeding and self-stimulation within the lateral hypothalamus of the rat.* PLoS One, 2020. **15**(1): p. e0224301.

54. Kornetsky, C., et al., *Intracranial Self-stimulation Thresholds: A Model for the Hedonic Effects of Drugs of Abuse.* Archives of General Psychiatry, 1979. **36**(3): p. 289-292.

55. Ausubel, D.P., *Note on a Threshold Concept of Reinforcement.* The Journal of General Psychology, 1965. **72**(2): p. 239-240.

56. Augier, E., et al., *A molecular mechanism for choosing alcohol over an alternative reward.* Science, 2018. **360**(6395): p. 1321-1326.

57. Berger, A.C. and J.L. Whistler, *Morphine-induced mu opioid receptor trafficking enhances reward yet prevents compulsive drug use.* EMBO Mol Med, 2011. **3**(7): p. 385-97.

58. O'Neal, T.J., et al., *Chemogenetic modulation of accumbens direct or indirect pathways bidirectionally alters reinstatement of heroin-seeking in high- but not low-risk rats.* Neuropsychopharmacology, 2020. **45**(8): p. 1251-1262.

59. Vanderschuren, L. and S.H. Ahmed, *Animal Models of the Behavioral Symptoms of Substance Use Disorders.* Cold Spring Harb Perspect Med, 2021. **11**(8).

60. Lüscher, C. and P.H. Janak, *Consolidating the Circuit Model for Addiction.* Annu Rev Neurosci, 2021. **44**: p. 173-195.

61. Harris, G.C. and G. Aston-Jones, *Altered Motivation and Learning Following Opiate Withdrawal: Evidence for Prolonged Dysregulation of Reward Processing.* Neuropsychopharmacology, 2003. **28**(5): p. 865-871.

62. Harris, G.C. and G. Aston-Jones, *Activation in extended amygdala corresponds to altered hedonic processing during protracted morphine withdrawal.* Behav Brain Res, 2007. **176**(2): p. 251-8.

63. Zhang, D., et al., *Morphine withdrawal decreases responding reinforced by sucrose self-administration in progressive ratio.* Addict Biol, 2007. **12**(2): p. 152-7.

64. Dalley, J.W., B.J. Everitt, and T.W. Robbins, *Impulsivity, compulsivity, and top-down cognitive control.* Neuron, 2011. **69**(4): p. 680-94.

65. Leyton, M. and P. Vezina, *Dopamine ups and downs in vulnerability to addictions: a neurodevelopmental model.* Trends Pharmacol Sci, 2014. **35**(6): p. 268-76.

66. Swain, Y., J.C. Gewirtz, and A.C. Harris, *Behavioral predictors of individual differences in opioid addiction vulnerability as measured using i.v. self-administration in rats.* Drug Alcohol Depend, 2021. **221**: p. 108561.

67. Vest, N., C.J. Reynolds, and S.L. Tragesser, *Impulsivity and risk for prescription opioid misuse in a chronic pain patient sample.* Addict Behav, 2016. **60**: p. 184-90.

68. Belin, D., et al., *High impulsivity predicts the switch to compulsive cocaine-taking.* Science, 2008. **320**(5881): p. 1352-5.

69. Tolomeo, S., et al., *Multifaceted impairments in impulsivity and brain structural abnormalities in opioid dependence and abstinence.* Psychological Medicine, 2016. **46**(13): p. 2841-2853.

70. Zhai, T., et al., *Nature of functional links in valuation networks differentiates impulsive behaviors between abstinent heroin-dependent subjects and nondrug-using subjects.* Neuroimage, 2015. **115**: p. 76-84.

71. Lee, T.M. and C.W. Pau, *Impulse control differences between abstinent heroin users and matched controls.* Brain Inj, 2002. **16**(10): p. 885-9.

72. Xie, C., et al., *Identification of hyperactive intrinsic amygdala network connectivity associated with impulsivity in abstinent heroin addicts.* Behav Brain Res, 2011. **216**(2): p. 639-646.

73. Mavrikaki, M., et al., *Chronic opioid exposure differentially modulates oxycodone self-administration in male and female rats.* Addict Biol, 2021. **26**(3): p. e12973.

74. Cooper, Z.D., et al., *Morphine deprivation increases self-administration of the fast- and short-acting mu-opioid receptor agonist remifentanil in the rat.* J Pharmacol Exp Ther, 2008. **326**(3): p. 920-9.

75. Townsend, E.A., et al., *Opioid withdrawal produces sex-specific effects on fentanyl-vs.-food choice and mesolimbic transcription.* Biol Psychiatry Glob Open Sci, 2021. **1**(2): p. 112-122.

76. Chaudhary, M.A., et al., *Development and Validation of a Bedside Risk Assessment for Sustained Prescription Opioid Use After Surgery.* JAMA Network Open, 2019. **2**(7): p. e196673-e196673.

77. Lanzillotta, J.A., et al., *The Impact of Patient Characteristics and Postoperative Opioid Exposure on Prolonged Postoperative Opioid Use: An Integrative Review.* Pain Management Nursing, 2018. **19**(5): p. 535-548.

78. McAuliffe, P.F., et al., *Second-hand exposure to aerosolized intravenous anesthetics propofol and fentanyl may cause sensitization and subsequent opiate addiction among anesthesiologists and surgeons.* Medical Hypotheses, 2006. **66**(5): p. 874-882.

79. Gold, M.S., J.A. Byars, and K. Frost-Pineda, *Occupational exposure and addictions for physicians: case studies and theoretical implications.* Psychiatric Clinics, 2004. **27**(4): p. 745-753.

80. Juurlink, D.N. and I.A. Dhalla, *Dependence and Addiction During Chronic Opioid Therapy.* Journal of Medical Toxicology, 2012. **8**(4): p. 393-399.

81. Fishbain, D.A., et al., *What percentage of chronic nonmalignant pain patients exposed to chronic opioid analgesic therapy develop abuse/addiction and/or aberrant drug-related behaviors? A structured evidence-based review.* Pain Med, 2008. **9**(4): p. 444-59.

82. Bravo, I.M., et al., *Divergent behavioral responses in protracted opioid withdrawal in male and female C57BL/6J mice.* Eur J Neurosci, 2020. **51**(3): p. 742-754.

83. Kosten, T.R., B.J. Rounsaville, and H.D. Kleber, *Ethnic and gender differences among opiate addicts.* Int J Addict, 1985. **20**(8): p. 1143-62.

84. Yu, J., et al., *Gender and stimulus difference in cue-induced responses in abstinent heroin users.* Pharmacol Biochem Behav, 2007. **86**(3): p. 485-92.

FIGURE LEGENDS

Figure 1. Viral translating ribosome affinity purification approach performed using MOR-Cre mice allows to sequence the transcriptome of DRN-MOR neurons. (A) Schematic of experimental timeline: MOR-Cre mice were injected in the DRN to express L10a-mCherry protein in DRN-MOR neurons, and were subsequently injected chronically either with saline CTL) or morphine (ABS). Four weeks after the last morphine exposure the DRN was micro-dissected. A fraction of total tissue mRNAs was conserved (input samples) and we immuno-precipitated mRNAs bounds to mCherry-L10a (IP samples) (n=6/6). **(B)** Principal component analysis: Factor 1 explains 41.7% of the variance of the and mostly corresponds to the fraction samples (IP vs input). **(C)** Quantification of Oprm1 transcripts: IP samples were enriched for Oprm1 transcripts compare to input samples for CTL and ABS. **(D)** Quantification of mCherry transcripts: IP samples were enriched for mCherry transcripts compare to input samples for CTL and ABS. Data are represented as mean ± SEM. *: $p<0.05$; **: $p<0.01$; ****: $p<0.0001$.

Figure 2. DRN-MOR neurons of abstinent mice show decreased gene expression related to opioids signaling and neuronal excitability. (A) Differentially expressed genes after morphine abstinence (CTL vs ABS) are mainly distinct genes in input vs IP samples. **(B)** Comparison of the fold change of differentially expressed genes in CTL vs ABS: the fold change of differentially expressed genes is higher in IP versus input samples. **(C)** Comparison of the fold change of differentially expressed genes in IP vs input for all genes or genes differentially expressed in IP CTL vs IP ABS: the fold change of differentially expressed genes were higher when looking only at genes affected by morphine abstinence (IP CTL vs ABS differentially expressed genes) than at all genes. **(D)** Over representation-analysis: the gene ontology (GO) terms underrepresented in DRN-MOR neurons of ABS animals included: Molecular function (passive transmembrane transporter activity, channel activity, cation channel activity, ion channel activity, substrate specific channel activity), Cellular component

(cilium, ciliary part, axoneme part) and Biological processes (metanephros development, kidney morphogenesis). **(E-F)** Gene Set Enrichment Analysis (GSEA) with gene set REACTOME_OPIOID_SIGNALLING [33]. **(E)** GSEA performed on IP ABS vs CTL differentially expressed genes indicated transcriptional depletion of opioid signaling pathway in DRN-MOR neurons of ABS animals. **(F)** Enrichment profile for differentially expressed genes between IP CTL vs ABS. Data are represented as mean ± SEM. *: p<0.05; ****: p<0.0001.

Figure 3. Control and abstinent mice learn to self-stimulate DRN-MOR neurons. (A) Schematic of the experimental timeline: MOR-cre mice were injected in the DRN to express mCherry-ChR2 proteins and implanted with an optic fiber to activate DRN-MOR neurons with laser stimulation. Three weeks after surgeries, mice were injected either with saline (CTL, n=17) or with escalating doses of morphine (ABS, n=17). Four weeks after the last injection, mice were trained to nosepoke for the laser stimulation according to a fixed ratio of 1 (FR1; 4 days), FR3 (9 days) and FR5 (15 days) (acquisition). Mice were also evaluated for different addiction-related behaviors (persistence to respond, motivation, compulsion and reinstatement after extinction training). **(B)** Left. Total number of nosepokes performed during each 1 hr self-stimulation session during acquisition (28 days). Right. Average nosepokes performed during each reinforcement schedule: CTL and ABS discriminated the active from the inactive and increased the number of active nosepoke according to the schedule. **(C)** Left. Total number of earned laser stimulation bouts during each self-stimulation session during acquisition. Left. Average laser stimulations earned during each reinforcement schedule: CTL and ABS mice earned similar number laser stimulation across schedules. Data are represented as mean ± SEM.**** / °°°°: p<0.0001.

Figure 4. Abstinent mice perform more impulsivity-like and persistent responses when evaluated for several addiction-related behaviors. (A) Left. Total number of impulsivity-like responses during each 1 hr self-stimulation session during acquisition (28 days. Right. Average impulsivity-like nose pokes per session for each reinforcement schedule: ABS mice

performed in average more impulsivity-like nose pokes during acquisition. **(B)** Left. Persistence to respond FR3: ABS mice performed more persistent nose pokes than CTL mice. Right. Persistence to respond FR5: ABS did not perform more persistent responses than CTL mice. **(C)** Motivation: ABS mice did not perform more active nose pokes during the progressive ratio session **(D)** Compulsivity-like: ABS mice did not earn more laser stimulation during the foot-shock session. **(E)** Extinction and reinstatement: cue presentation reinstated active nose pokes after extinction in CTL and ABS mice. Data are represented as mean ± SEM. #: $p<0.05$; **: $p<0.01$; **** / °°°°: $p<0.001$.

Figure 5. Abstinent mice score higher for addiction-related criteria in the oICSS behavior. (A-C) Comparison of addiction-related behaviors in mice presenting 0, 1, 2 or 3 criteria of addiction-related behaviors. The higher the criteria of addiction-related behavior the higher the animal scored for **(A)** the persistence to respond **(B)** the motivation **(C)** the compulsivity-like responses. **(D)** % of mice in each criterion of addiction-related behaviors for CTL and ABS mice. **(E)** ABS mice have higher criteria of addiction-related behaviors than CTL mice. **(F)** Principal component analysis: Factor 1 explains 45.3% of the total variance between individuals and takes into account four behavioral measures (compulsivity, motivation, persistence to respond and reinstatement). **(G-H)** Representation of individual values in Factor 1 and 2 according to **(G)** the group-criteria of addiction-related behaviors: Factor 1 ranks the individuals according to their criteria of addiction-related behavior. **(H)** the treatment: Factor 1 ranks the individuals according to their treatment (morphine or saline). Data are represented as mean ± SEM. *: $p<0.05$; **: $p<0.01$; ***: $p<0.001$; ****: $p<0.0001$.

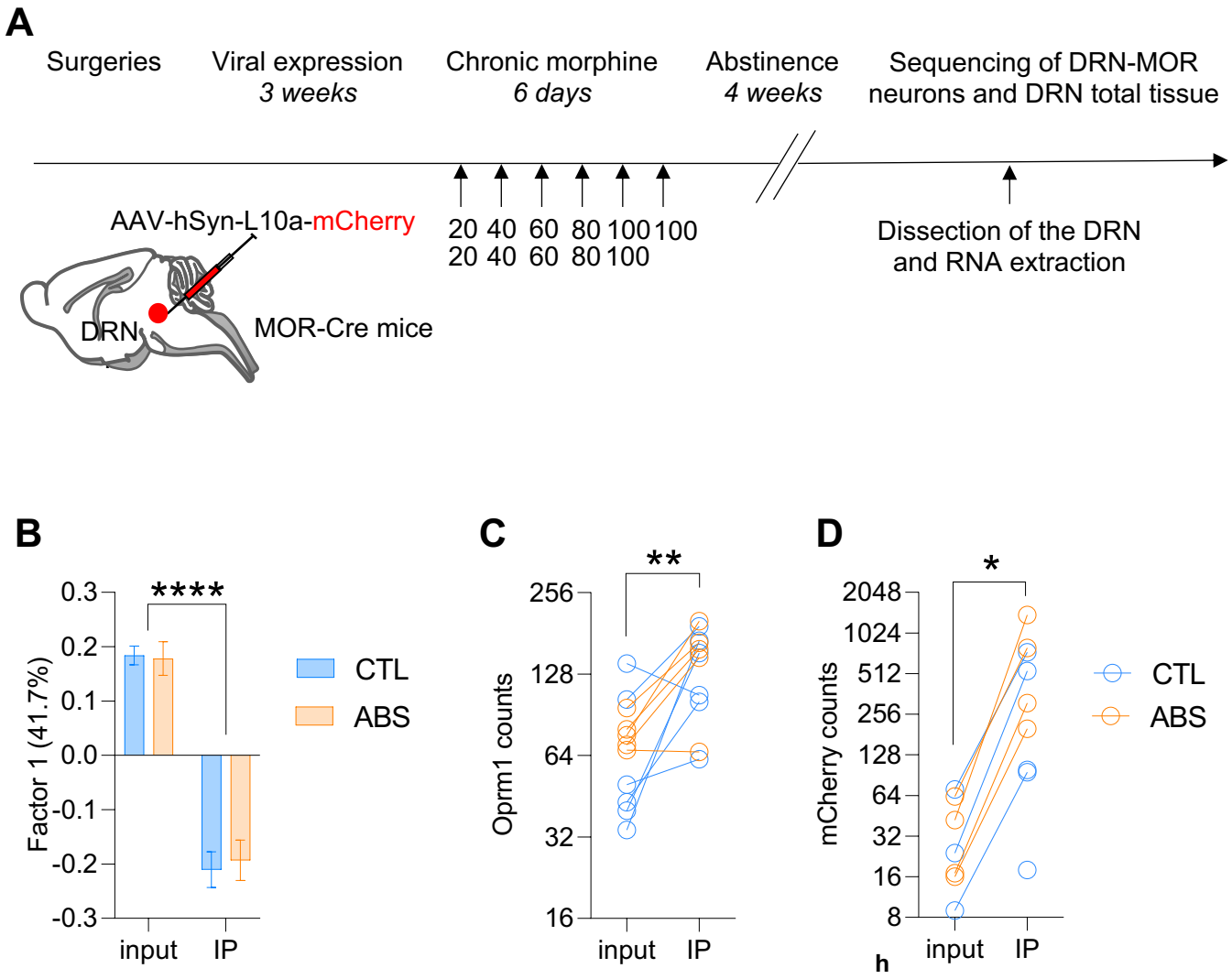

Figure 1. Welsch et al

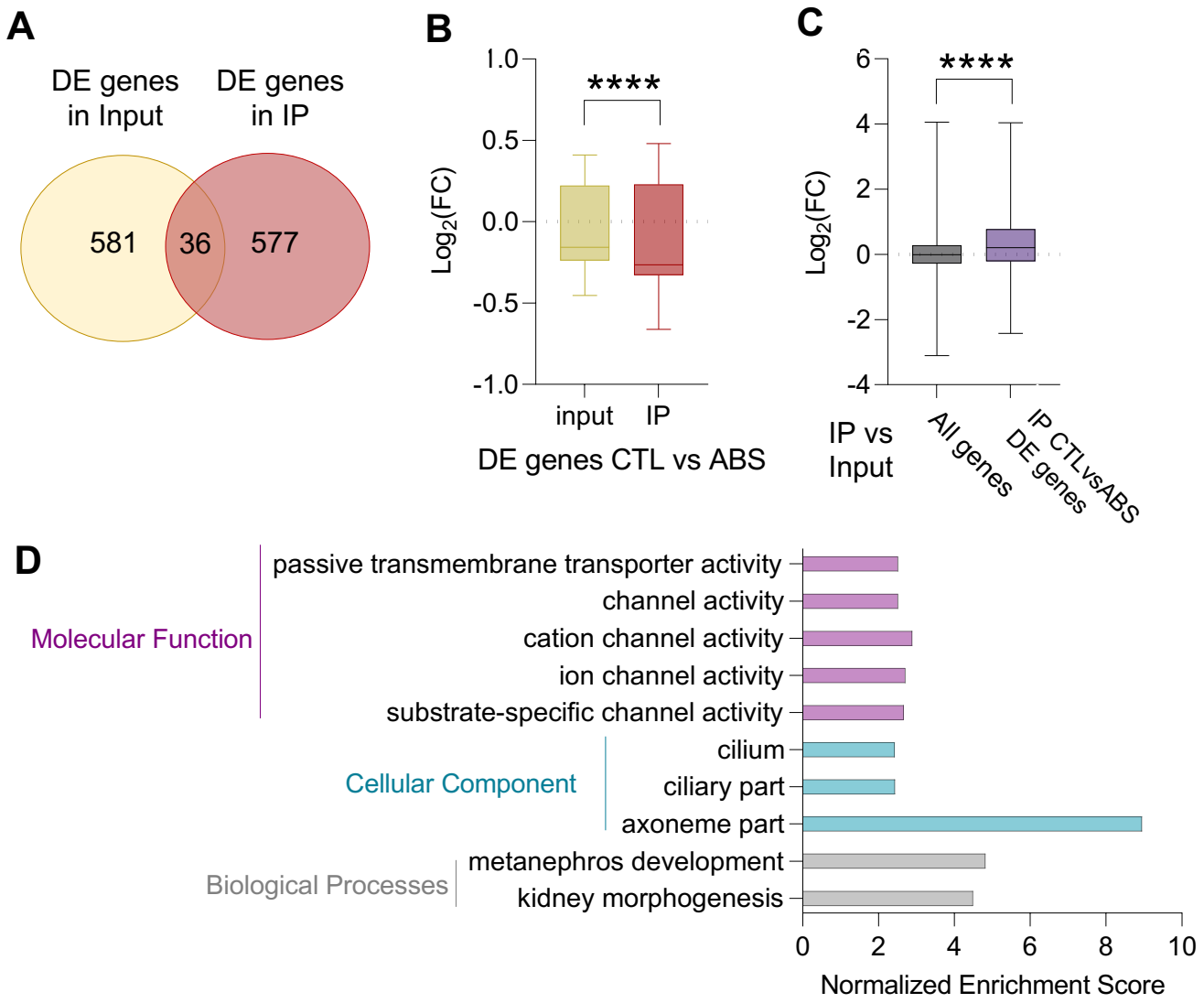

Figure 2. Welsch et al

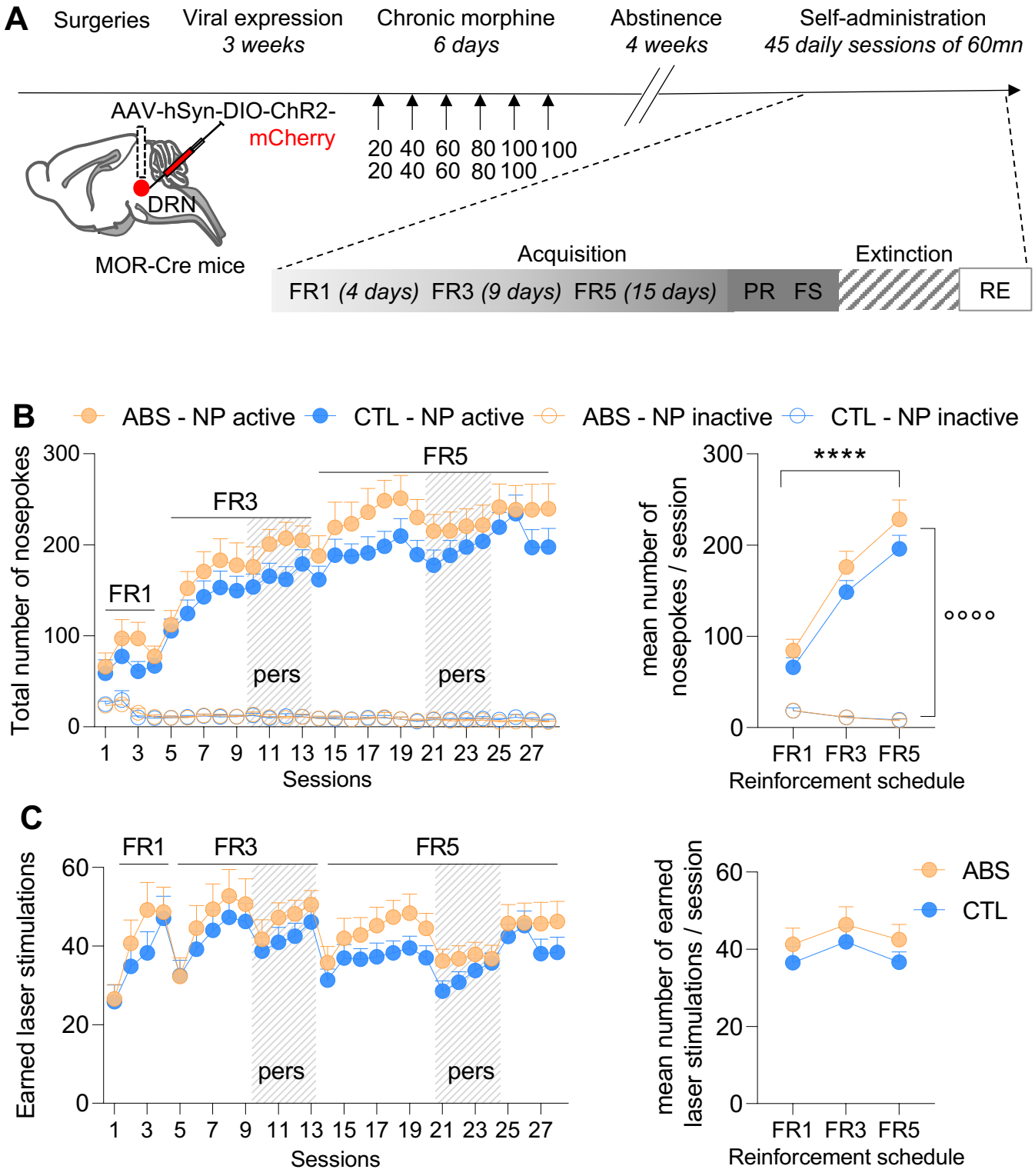

Figure 3. Welsch et al

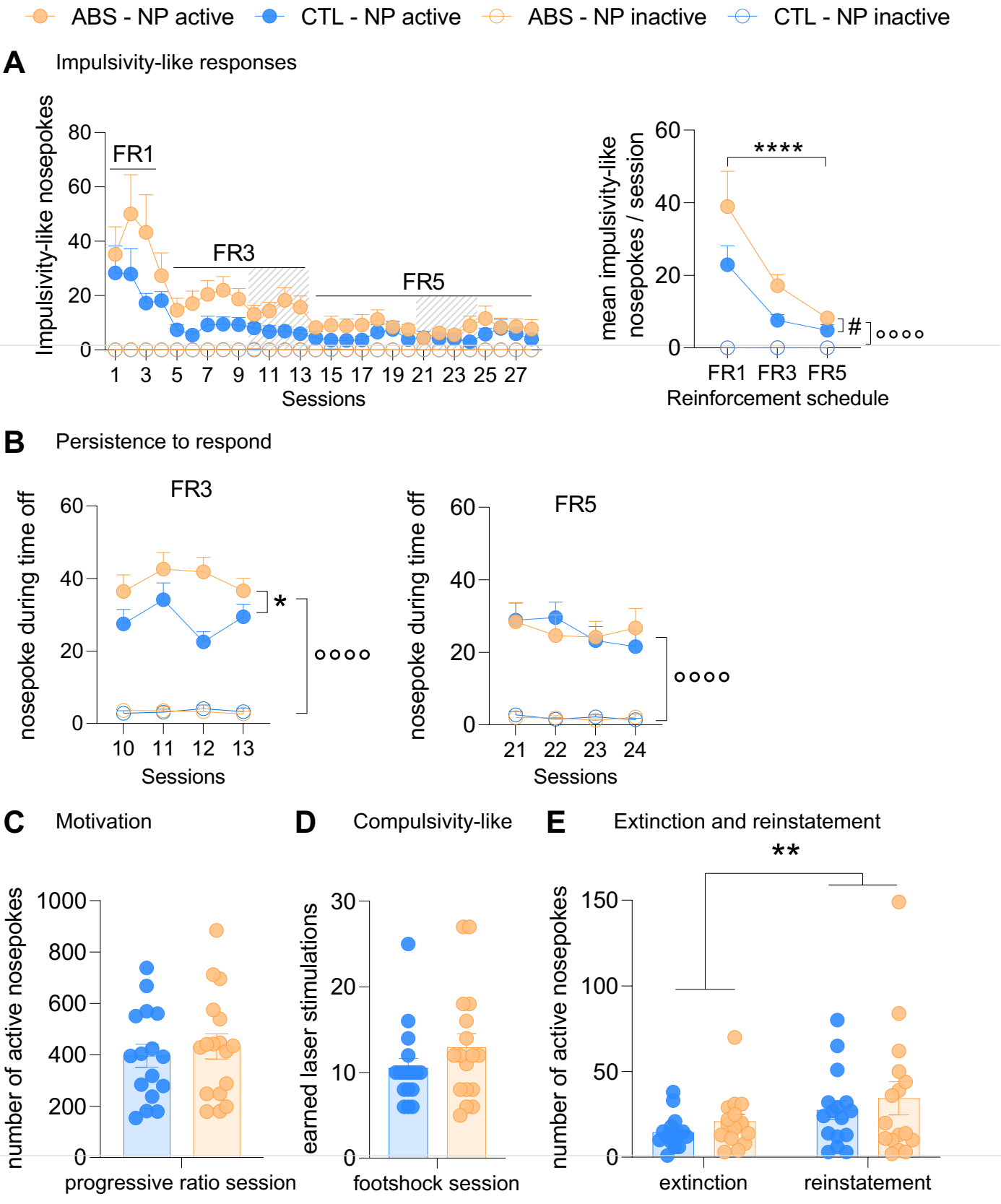

Figure 4. Welsch et al

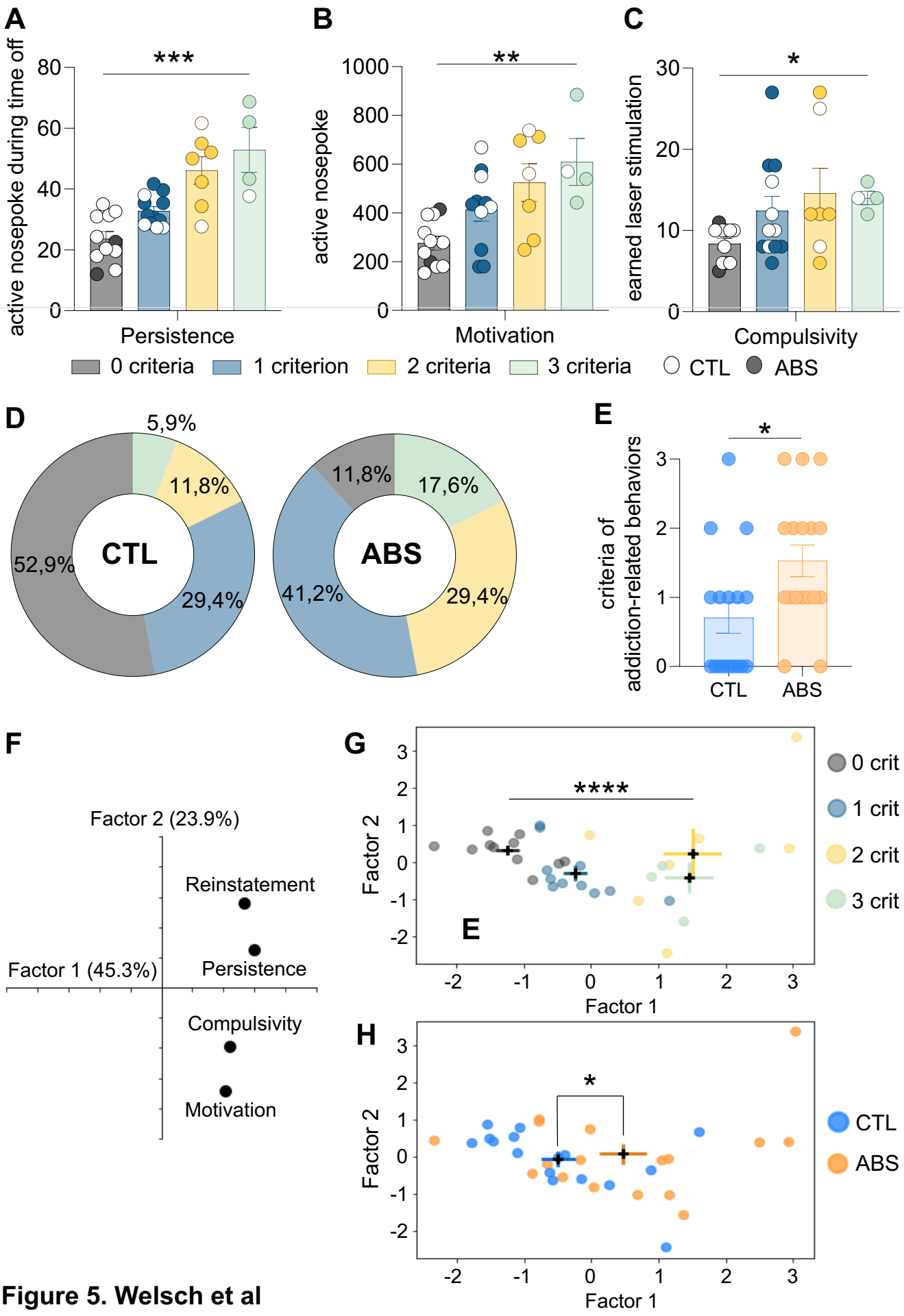

Figure 5. Welsch et al

Mu opioid receptor-positive neurons in the dorsal raphe nucleus are impaired by morphine abstinence

Lola Welsch[1,2], Esther Colantonio[2], Camille Falconnier[3], Florence Allain[2], Sami Ben Hamida[4], Emmanuel Darcq[2], Pierre-Eric Lutz[3] and Brigitte L. Kieffer[1,2]

1: Douglas Research Center, Department of Psychiatry, McGill University, Montréal, Quebec H4H 1R3, Canada

2: INSERM U1114, Department of Psychiatry, University of Strasbourg, Strasbourg 67084, France

3: Centre National de la Recherche Scientifique, Université de Strasbourg, Institut des Neurosciences Cellulaires et Intégratives UPR3212, 67000 Strasbourg, France

4: . INSERM UMR 1247, Université de Picardie Jules Verne, Amiens, France

Corresponding author:

Brigitte L. Kieffer, INSERM U1114 University of Strasbourg, CRBS 1 rue Eugène Boeckel, CS60026 67084 Strasbourg Cedex France

brigitte.kieffer@unistra.fr

Short title (55 characters): Effects of morphine abstinence on DRN-MOR neurons

Keywords: opioids, dorsal raphe nucleus, abstinence, addiction-related behaviors, opto-intracranial self-stimulation, vTRAP-seq

SUPPLEMENTARY METHODS AND MATERIALS

Stereotaxic surgery and viruses

Animals were anesthetized in an induction chamber with 5% isoflurane for five minutes and maintained at 1-2% isoflurane during the whole procedure. For viral injection, a stereotaxic frame (Kopf) and a nanoinjecter (Drummond) was used to deliver 500nL of virus in the DRN (AP: -4,15, ML: 0; DV: -3,4). For mice receiving intracranial implants, optogenetic optical fibers (Newdoon, 200µm NA: 0.37) were implanted above the DRN injection site (AP: -4,15, ML: 0; DV: -3,3). Implants were secured with two layers of Metabond (C&B Metabond). Depending on the experiment, the following viruses were used: AAV2-hsyn-DIO-ChR2-mCherry (ChR2), AAV2-hSyn-DIO-mCherry (control), AAV2-hsyn-flex-RPL10a-mCherry (RNAseq). After surgery, mice were injected with the analgesic Meloxicam (Metacam, mg/kg). Handlings and experiments started ~28 days after surgeries to allow mice to recover and the virus-mediated expression of transgenes.

Morphine treatment

According to a procedure from [1], mice were injected i.p. twice daily with escalating doses of morphine (20, 40, 60, 80, 100 mg/kg for 5 days, followed by a single 100mg/kg injection on day 6) at a volume of 10mL/kg. In parallel, a control group was injected with saline i.p. following the same schedule. Mice were housed with individuals receiving the same treatment (morphine- or saline-only). After the chronic morphine treatment, mice were undisturbed and maintained drug-free for four weeks prior to further experimentations (brain dissection, operant self-administration).

RNA sequencing

RNA extraction

DRN dissection was performed at 4 weeks of abstinence on MOR-Cre mice that have been previously injected with a vTRAP Cre-dependent virus [2] in the DRN and submitted to the morphine treatment. Mice were decapitated and the DRN was quickly manually dissected using punch (2mm diameter collected on 2 slices of 200 µm width). As the DRN is a relatively small brain region, the tissue of four mice were pooled for one sample. To obtain six samples per group, a total of 48 mice (morphine and control) have been used. Translated mRNA purification has been made following [3, 4]. Pooled DRN tissue was immediately emerged in a pre-chilled tissue-lysis buffer (20mM HEPES KOH [pH 7.3], 150mM KCL, 12mM MgCl2, 1M DTT, 100µg/mL cycloheximide, protease inhibitors, and RNase inhibitors) and homogenized using a homogenizer (Fisher Scientific). To remove large cells debris, the homogenates were centrifuged at 2000 x g, 4°C for 10min and NP-40 (1%) and DHPC (30mM) were added to the supernatant. After 5min incubation on ice, the lysate was centrifuged at 20000 x g to remove unsolubilized material and the supernatant was collected. In parallel, mCherry antibodies coupled to magnetic beads were washed three times in low-salt buffer (HEPES KOH [7.3pH], 150mM KCl, 12mM MgCl2, 0.5mM DTT, 100µg/mL cycloheximide). Before adding the magnetic beads to precipitate mCherry-coupled mRNA transcripts, 250µL of the total tissue lysate is collected to separate the transcriptome of the total DRN tissue from the transcriptome of MOR+ cells. Then, 200µL of freshly prepared magnetic beads were added to each samples and were incubated overnight at 4°C under end-over-end agitation. After incubation, beads were collected on a pre-chilled magnetic rack and washed four times with high salt buffer (HEPES KOH [7.3pH], 350mM KCl, 12mM MgCl2, 1% NP-40, 0.5mM DTT, 100µg/mL cycloheximide). All the remaining washing buffer was subsequently removed and beads were resuspended in nanoprep lysis buffer (20mM HEPES KOH [pH 7.3], 150mM KCL, 12mM MgCl2, 1M DTT, 100µg/mL cycloheximide, protease inhibitors, RNase inhibitors and β-mercaptoethanol). RNA transcripts were separated from the beads after thorough vortexing and 10min incubation at room temperature. RNA extraction was performed on total tissue and immuno-precipitated fractions for each samples by adding an equal volume of 80% sulfolane and following the protocol from the Absolutely Nanoprep kit (Agilent), including the extra DNAse treatment step. The extracted RNA were stored at -80°C until sequencing.

RNA sequencing, library preparation and mapping

The step described below were carried out by the GenomEast platform at the Institute of Genetics and Molecular and Cellular Biology. *Library preparation:* it was performed using Clontech SMART-Seq v4 Ultra Low Input RNA Kit for Sequencing User Manual – PN 091817 + Illumina Nextera XT DNA Library Prep Kit Reference Guide - PN 15031942. Full length cDNA were generated from 0.5 ng of total RNA using SMART-SeqX v4 UltraX Low Input RNA Kit for Sequencing (Takara Bio Europe, Saint Germain en Laye, France) according to manufacturer's instructions with 12 cycles of PCR for cDNA amplification by Seq-Amp polymerase. Six hundreds pg of pre-amplified cDNA were then used as input for Tn5 transposon tagmentation by the Nextera XT DNA Library Preparation Kit (96 samples) (Illumina, San Diego, USA) followed by 12 cycles of library amplification. Following purification with SPRIselect beads (Beckman-Coulter, Villepinte, France), the size and concentration of libraries were assessed by capillary electrophoreris. *Sequencing*: Libraries were sequenced on an Illumina HiSeq 4000 sequencer as single read 50 base reads. *Mapping*: Reads were mapped onto the mm10 assembly of *Mus musculus* genome using STAR version 2.5.3a. *Quantification*: Gene expression quantification was performed from uniquely aligned reads using htseq-count version0.6.1p1, with annotations from Ensembl version 102 and “union” mode. Only non-ambiguously assigned reads to a gene have been retained for further analyses. *Batch effect correction*: ComBat-Seq was used to adjust batch effect and the resulting matrix was used in DESeq2 (version RNA-seq analysis 1.16.1) [5].

RNA-seq analyses

Principal component analysis (PCA): The gene expression profiles (normalized transcripts counts for all genes expressed in our samples) of each sample were used to perform a PCA, that identified factors (or principal components) which best explained the variance between the samples. The groups (IP and input for CTL and ABS) were identified, plotted and compared in the axis defined by Factor 1.

Over-Representation analysis (ORA): The WebGestalt web-based software [6] was used for gene ontology analyses: it was performed on differentially expressed (DE) genes between IP ABS vs CTL ($p<0.05$, unpaired t-test). All genes detected in the comparison IP between input served as reference gene list. The false discovery rate (FDR) was calculated using the Benjamini-Hochberg (BH) correction for multiple testing. All genes identified are available as Supplementary tables (**Suppl Table 1-5**)

Gene set enrichment analysis (GSEA): Genes were ranked according to their log2 fold change ($Log_2(FC)$) and this ranking was entered into GSEA software [7] to run pre-ranked GSEA on all pertinent comparisons. Enrichment was compare to the gene set englobing all genes expressed in different DRN cell types (mean genes expression >0.7, from [8]) opioid signaling cascade [9]. The FDR was calculated using the BH correction for multiple testing. All results are available in **Supplementary Table 6**.

Operant optogenetic self-stimulation

Animal preparation

MOR-cre mice were injected with a cre-dependent virus expressing either mCherry only (n=4) or ChR2 fused with mCherry (n=35). Three weeks after stereotaxic surgery, mCherry- and ChR2-mice were either submitted to the chronic morphine treatment or to saline injections. mCherry-mice treated with saline (n=2) or morphine (n=2) were combined together since statistical analysis showed no difference, and are referred as mCherry (n=4). Mice expressing the ChR2 and treated with morphine are referred as ABS (n=18) and mice expressing the ChR2 and treated with saline are referred as CTL (n=17). The self-stimulation procedure started 4 weeks after morphine abstinence. All experiments were conducted during the light phase.

Acquisition

Daily self-stimulation sessions were conducted in operant chamber (iMetronic) composed of 2 nosepoke ports (one active and one inactive, counterbalanced across animals) and lasted 60min with no maximum of reward. Each laser-stimulation (LS) was delivered following this schedule (**Suppl Figure 4**): nosepoking in the rewarded active nosepoke resulted in 10s of a cue-light, and 5s LS was delivered 5s later (after nosepoke) for 15s. The LS was delivered as 30 bursts of 5 laser pulses (each burst consists in 5ms at 20Hz, 5mW) separated by 250 ms, see [10]. Each active nosepoke was followed by a 20s timeout period where nosepoking had no consequence but was recorded. During the first four sessions, the reward delivery followed a fixed ratio one (FR1; sessions 1-4), then a FR3 (sessions 5-13) and FR5 (sessions 14-28) schedules were performed (**Fig 3A**). **Acquisition criteria:** As described previously [11, 12], we considered that mice achieved acquisition when the following conditions were met: (1) mice maintained a stable responding to earn a number of reinforcers with less than 20% deviation from the mean in 3 consecutive sessions (2) at least 75% of nosepokes were made in the active port and (3) mice earned at least 5 reinforcers per session. Mice that did not meet the acquisition criteria were excluded from the analyses. For DRN-MOR neurons oICSS: 1 ABS mouse was excluded (1/18), none of the CTL mice was excluded (0/17), and as expected none of the mCherry-mice acquired the SA (4/4). For sucrose SA: 6 mice did not meet the acquisition criteria and were excluded from analysis (6/19).

Persistence to respond

During the FR3 and FR5 acquisition sessions, 4 sessions (FR3: sessions 10-13; FR5: sessions 21-24) were used to measure persistence to respond. These sessions were composed of two LS periods of 25min where the LS was available, separated by one time-off period of 10min where the reward was not available (nor the cue light). The time-off period was signaled by turning off the house light (same signal as for the end of the session also indicating the end of LS availability). To evaluate the persistence to respond, the number of active responses during the time off period were scored during the 3 last sessions of FR3 (sessions 11-13).

Progressive Ratio

After the 28 days of SA acquisition, the motivation of the mice to obtain the LS was evaluated using a single progressive ratio session. The response required to earn a LS progressed as following: 1, 3, 5, 8, 12, 16, 22, 29, 38, 50, 65, 84, 108, 139, 178. The progressive ratio session ended after 4 hours or if 1 hour elapsed since the last reinforced schedule has been reached [10, 13]. The motivation was measured as the total number of nosepokes performed during the progressive ratio session.

Punishment sessions

After the progressive ratio session, 2 additional SA sessions under FR5 schedule were performed in order to restore the baseline active responding. For the punishment session, mice were under the FR5 schedule of reinforcement as the day before but every third LS was coupled with a foot shock (500ms, 0.2mA) starting immediately after the rewarded nosepoke along with the light-cue and 5s before the onset of the LS. In addition, a new sound cue (1s, 2.5kHz) was paired with the nosepoke preceding the foot shock (the fourth nosepoke of the FR5) to warn that the next nosepoke will trigger the foot shock [10]. Compulsivity was measured as the number of LS earned during the punishment session.

Extinction and reinstatement

After the punishment session, 3 additional self-stimulation sessions in the FR5 schedule were performed to re-establish the baseline active responding. Then mice underwent extinction training sessions wherein active nosepokes had no consequence (no cue nor LS were delivered). After 10 days of extinction, mice were tested for cue-induced reinstatement: 3s after the beginning of the SA session, the light cue previously associated with the LS was presented to the mouse. Then, active nosepokes under a FR5 schedule for DRN-MOR neurons oICSS resulted in cue-light activation but the reward delivery was omitted. The timeout period, wherein nosepoking had no consequence, was reduced to 10s (the duration of the cue presentation).

Reinstatement was measured as the number of active nosepokes made in the cue-induced reinstatement session [14].

Attribution of the three addiction-like criteria

According to the analysis from [12, 15], each individual was attributed addiction-like criteria depending on their score in 1. the persistence to respond in acquisition sessions, 2. the progressive ratio session and 3. the punishment session. For the analysis, all individuals from CTL and ABS group were pooled and analyzed together. An animal was considered to be positive for one addictive-like criterion when responses in one of these sessions was in the 34^{th} highest percentile of the distribution. The score (0 or 1) obtained for each of the three evaluated addictive-like behaviors were summed and animals were separated into four groups ranging from 0 to 3 criteria. Then the proportion of animals treated with either saline or morphine in each criteria group was calculated.

Principal component analysis

The principal component analysis took into account 1. the persistence to respond in acquisition sessions, 2. the motivation to obtain the LS in the progressive ratio session, 3. the compulsive-like behavior in the punishment session and 4. the propensity to reinstate nosepoking after cue-light presentation in the reinstatement session. The 4 dimensions of the data (saline and morphine group pooled) were reduced with a standard principal component analysis (PCA), which identified factors (or principal components) computed according to the variance of the data. The data were then projected onto a new space created according to the axes defined by the two first factors, which best explain the variance. Once PCA was performed, the groups (either the numbers of addictive-like criteria, 0 to 3, or CTL/ABS) were identified, plotted and compared in the newly defined space.

Statistical analysis

All data were presented as mean ± standard error mean (s.e.m). Statistical significance is indicated as *: $p<0.05$, **: $p<0.01$ and ***: $p<0.001$. According to the experiments, t-test (paired or unpaired), one-way, two-way or three-way repeated measure ANOVA, Kruskal-Wallis and trend for Chi-square were used, followed when appropriate by a Bonferroni post-hoc, were used. Statistical analyses were performed using Graphpad Prism 9.3.1. For each experiment, the detailed statistics are available as supplementary tables (**Table 7-10**) and the group size are described in the corresponding figure legend.

Tissue preparation & image acquisition

At the end of each experimental procedure, unless otherwise noted, mice were deeply anesthetized with i.p. injection of a ketamine-xylazine cocktail and transcardially perfused with ~10mL 1X phosphate-buffered saline (PBS; Invitrogen, Thermo Fischer Scientific) and then ~50mL 4X paraformaldehyde (PFA; Electron Microscopy Science) using a peristaltic pump at 10mL/min. Brains were dissected and postfixed overnight in 4X PFA, cryoprotected for 48h in 30X sucrose solution (Thermo Fisher Scientific), embedded in OCT (Fischer Scientific) and frozen at -80°C. Brains were sliced (30µm coronal slice) using a cryostat (Leica) and stored in 1X PBS prior to immunohistochemistry. For injection site and optic fiber placements confirmation, an Olympus IX73 epifluorescence microscope with a 10X objective was used. For mouse cohorts used in behavioral experiments, the position of the viral injection site and the optic fiber placement were carefully confirmed before inclusion in the datasets.

SUPPLEMENTARY FIGURES

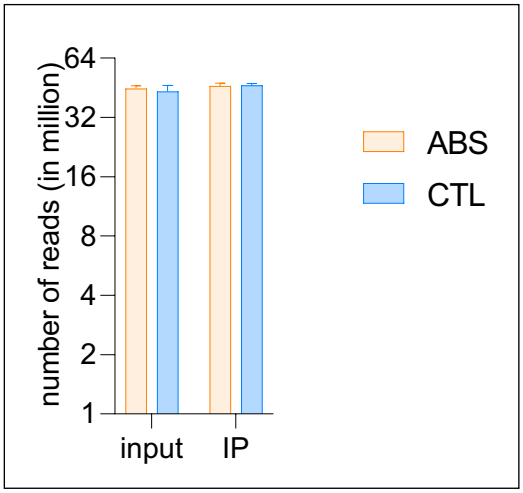

Supplementary Figure S1. Number of reads (in million) for each fraction (IP or input) and each treatment (CTL and ABS). All samples generated for transcriptomic analyses were sequenced at similar depth.

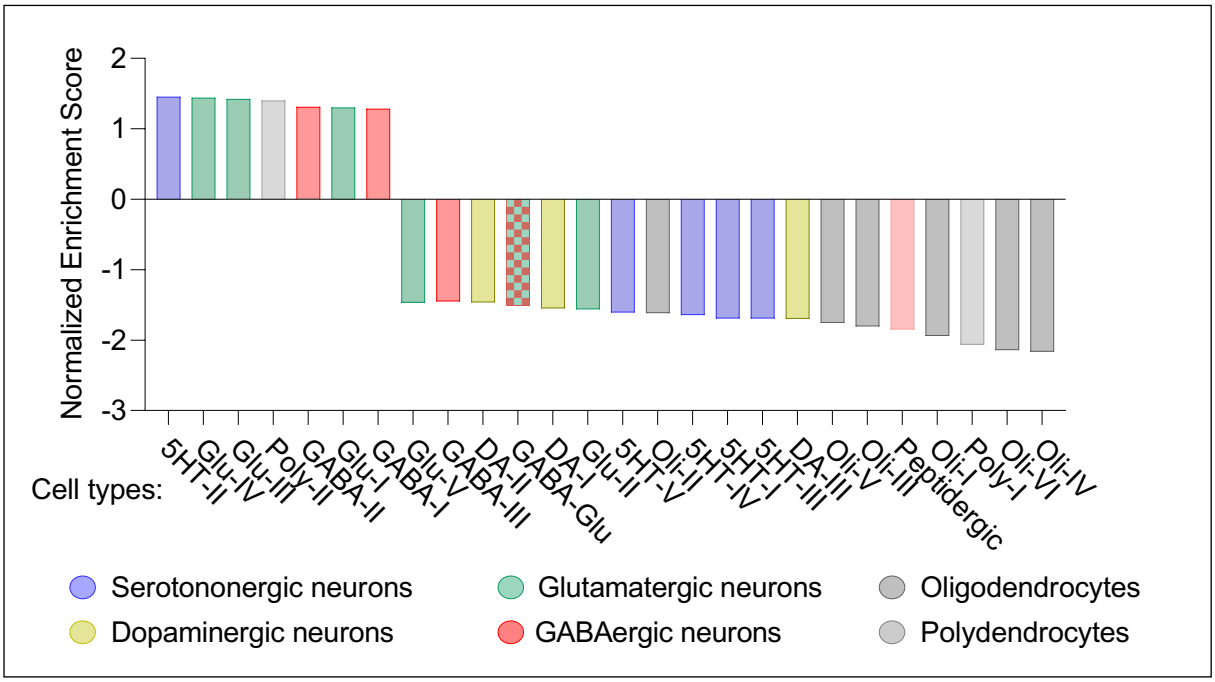

Supplementary Figure S2. Transcriptomic profile of DRN-MOR neurons match transcriptomic profiles of several DRN-neurons population.

Using Gene Set Enrichment Analysis, we compared single-cell mRNA sequencing from the DRN [8] to DE genes in IP vs input samples (genes enriched in DRN-MOR neurons). This analysis revealed that IP samples were enriched for presumed cell markers of a single type of serotonergic neurons (type II: located in vl-DRN and expressing notably *Hcrtr1/Asb4*), three types of Glutamatergic neurons (type IV: dm-DRN, *Slc17a8/Gata3*, III: near vl-PAG, *Pax6/Penk*, I: near vl-PAG, *Fign/Pdyn*), Polydendrocytes (type II: renewing, *Pdgfra/Top2a*) and two types of GABAergic neurons (type II: near vlPAG, *Kit/Ebf3*, type I: dl-DRN, *Asic/Calb2*). Conversely, they were depleted for presumed cell markers of oligodendrocytes (all types), dopaminergic neurons (all types), polydendrocytes (type I: quiescent, *Pdgfra/Cspg5*), peptidergic neurons, neurons co-expressing GABA-Glu, and every other types of glutamatergic, serotonergic and GABAergic neurons.

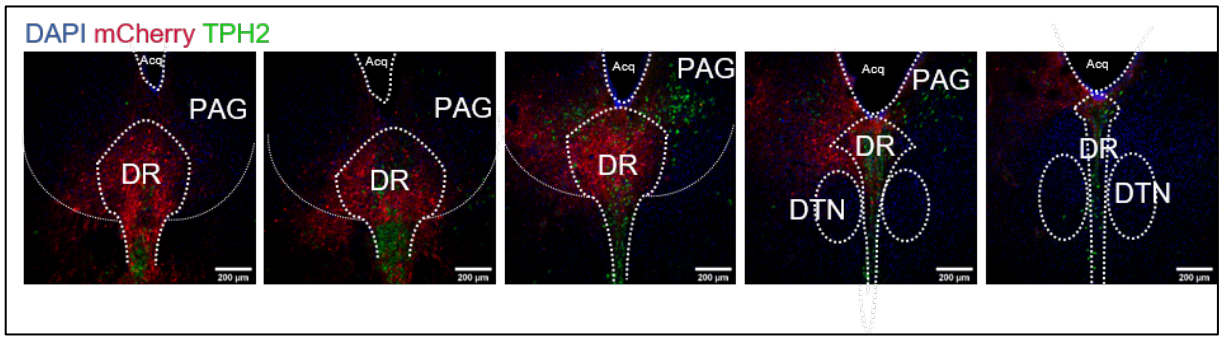

Supplementary Figure S3. Pattern of mCherry-expression in the DRN of MOR-Cre mice injected with cre-dependent virus. Immunochemistry was performed post-mortem for each individual in order to ensure accurate viral expression in the DRN. This image shows expression of the reporter gene (mcherry) across sections covering the DRN. Most of the staining is restricted to the DRN with limited expression in the PAG.

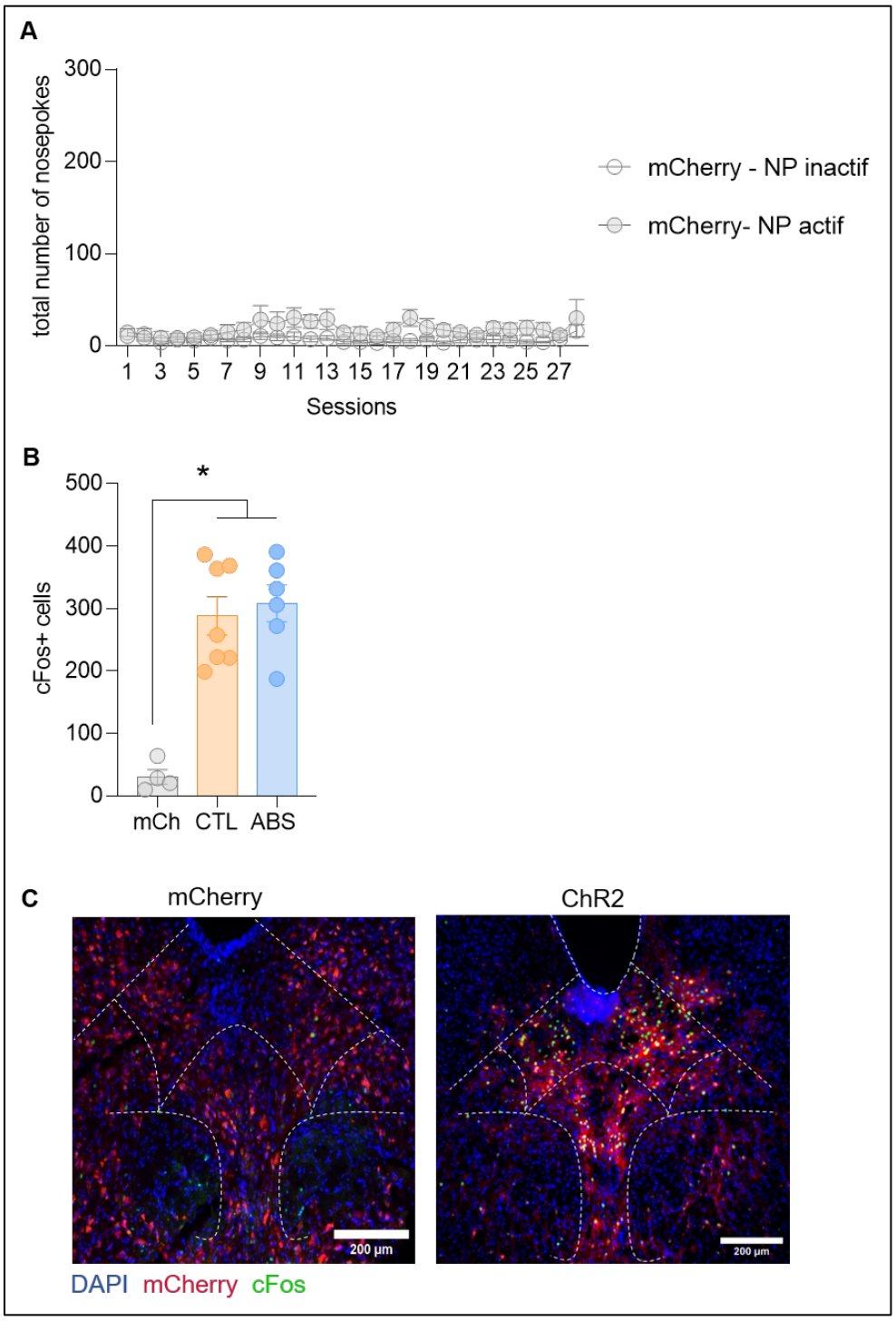

Supplementary Figure S4. mCherry-MOR-Cre mice did not self-administer the laser stimulation. (A) Total number of nosepokes performed during each 1 hr self-stimulation sessions during acquisition (28 days) (n=4) by mice expressing mCherry in the DRN. mCherry mice followed the same protocol described in **Figure 3A**. Mice treated with saline and morphine were pooled because no significant difference was detected between the groups. mCherry mice did discriminate between active and inactive nosepoke. **(B)** Quantification of c-fos-positive cells upon LS in the DRN of mice expressing either the control virus (mCh) or the ChR2-virus (CTL and ABS) (n=3-4): mice expressing the ChR2-virus had a ~10X fold increase expression of cFos compared to mice expressing mCherry-virus. **(C)** Representative cFos expression in the DRN of mCherry- and ChR2-expressing mouse upon LS.

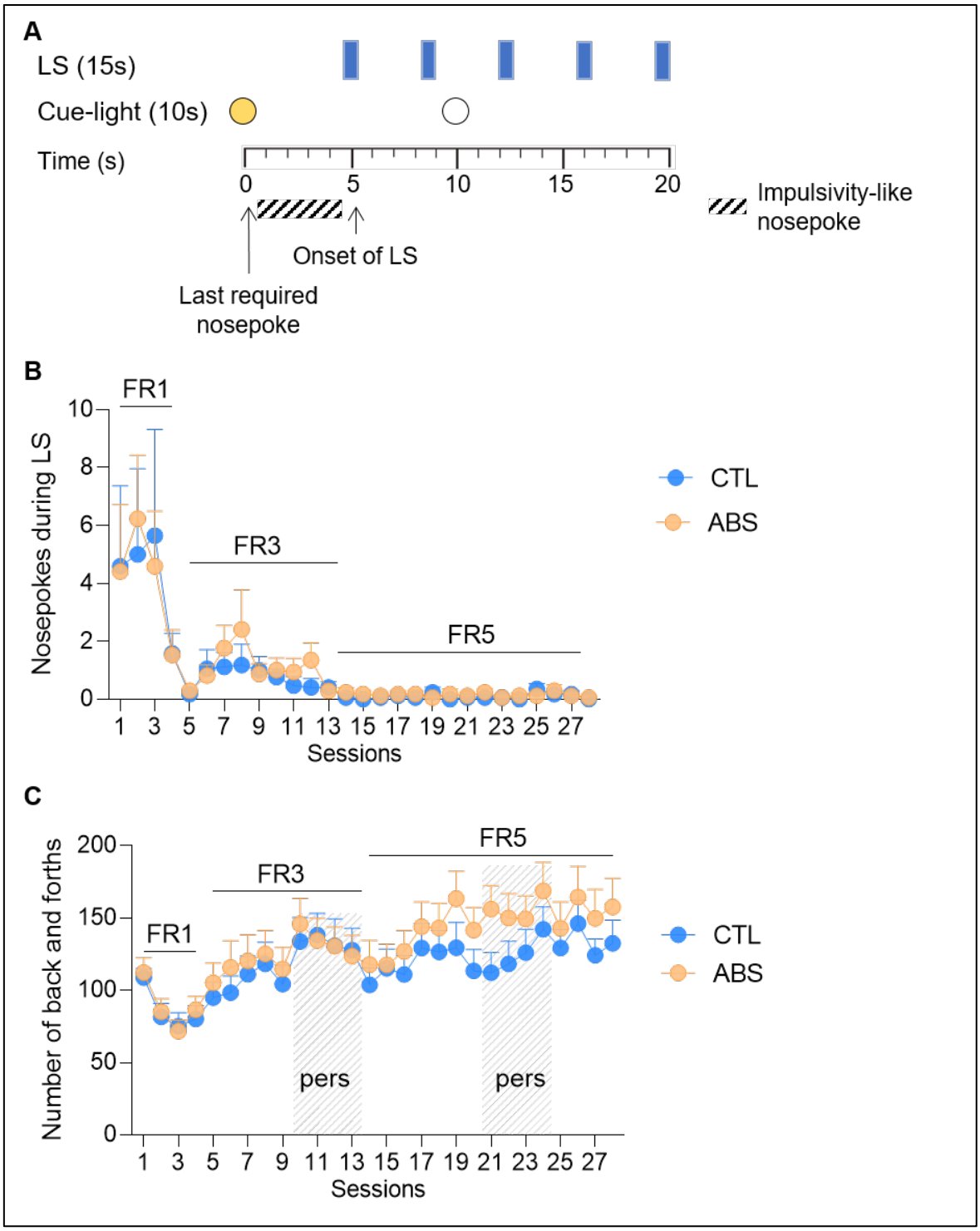

Supplementary Figure S5. Impulsive-like nosepokes during acquisition of oICSS. (A) Schematic of laser stimulation (LS) delivery schedule (adapted from [10]). After the last active nosepoke has been performed, the cue-light above the active nosepoke port turned on for 10s. 5s after the nosepoke, the LS starts for 15s (5 laser pulses of 4ms pulse width at 20Hz). Active nosepokes performed during the 5s delay between the active nosepoke and the onset of the LS are considered impulsive-like responses. **(B)** Number of nosepokes performed during the 15 s of LS along acquisition sessions: no significant difference between CTL and ABS (two-way RM ANOVA, Treatment effect, p=0.1501). **(C)** Number of back and forths performed during each acquisition session: no significant difference between CTL and ABS (two-way RM ANOVA, Treatment effect, p=0.42).

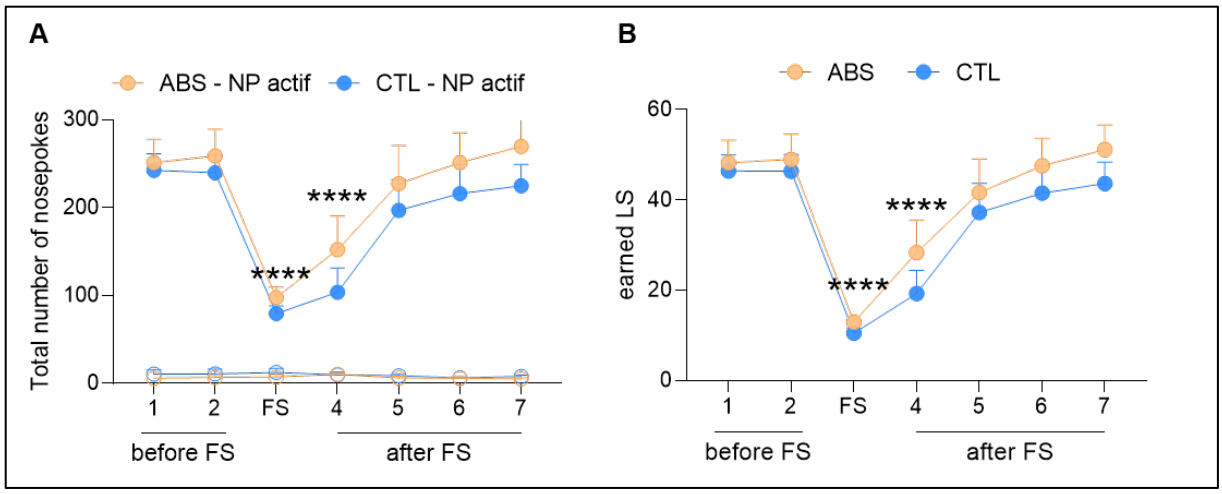

Supplementary Figure S6. Effect of footshock (FS) on nosepokes and earned LS. FS significantly decreased (two-way RM ANOVA, Session effect, $p<0.0001$) for both **(A)** nosepokes (****: $p<0.001$) and **(B)** earned LS (****: $p<0.0001$), and mice went back to their baseline nosepokes (****: $p<0.001$) and earned LS (****: $p<0.001$) at session 5 (the second session after FS). No significant difference between CTL and ABS neither for nosepokes (two-way RM ANOVA, Treatment effect, $p=0.382$), nor LS (two-way RM ANOVA, Treatment effect, $p=0.422$).

SUPPLEMENTARY TABLES

Supplementary Table S1. GO term: Ion channel activity. ID: 0005261; size=366; overlap=27; Enrichment Ratio=2.71; p=2.803e-6; FDR=1.099e-2.

Gene Symbol	Gene Name	Entrez Gene
Abcc8	ATP-binding cassette. sub-family C (CFTR/MRP). member 8	20927
Gabra3	gamma-aminobutyric acid (GABA) A receptor. subunit alpha 3	14396
Kcnk6	potassium inwardly-rectifying channel. subfamily K. member 6	52150
Kcns2	K+ voltage-gated channel. subfamily S. 2	16539
Clic6	chloride intracellular channel 6	209195
Tspoap1	TSPO associated protein 1	207777
Cacna1d	calcium channel. voltage-dependent. L type. alpha 1D subunit	12289
Trpc7	transient receptor potential cation channel. subfamily C. member 7	26946
Abcc9	ATP-binding cassette. sub-family C (CFTR/MRP). member 9	20928
Lrrc8c	leucine rich repeat containing 8 family. member C	100604
Scn4b	sodium channel. type IV. beta	399548
Htr3a	5-hydroxytryptamine (serotonin) receptor 3A	15561
Anxa2	annexin A2	12306
Itpr2	inositol 1.4.5-triphosphate receptor 2	16439
Trpc1	transient receptor potential cation channel. subfamily C. member 1	22063
Kcnmb4	potassium large conductance calcium-activated channel. subfamily M. beta member 4	58802
Cacng3	calcium channel. voltage-dependent. gamma subunit 3	54376
Cacng5	calcium channel. voltage-dependent. gamma subunit 5	140723
Tmem63c	transmembrane protein 63c	217733
Kcnip3	Kv channel interacting protein 3. calsenilin	56461
Kcnn4	potassium intermediate/small conductance calcium-activated channel. subfamily N. member 4	16534
Pex5l	peroxisomal biogenesis factor 5-like	58869
Panx1	pannexin 1	55991

Vdac1	voltage-dependent anion channel 1	22333
Best2	bestrophin 2	212989
Itpr1	inositol 1,4,5-trisphosphate receptor 1	16438
Kcnj14	potassium inwardly-rectifying channel. subfamily J. member 14	211480

Supplementary Table S2. GO term: Cation channel activity. ID: 0005261; size=280; overlap=22; Enrichment Ratio=2.89; p=8.768e-6; FDR=1.836e-2.

Gene Symbol	Gene Name	Entrez Gene
Abcc8	ATP-binding cassette. sub-family C (CFTR/MRP). member 8	20927
Kcnk6	potassium inwardly-rectifying channel, subfamily K, member 6	52150
Kcns2	K+ voltage-gated channel, subfamily S, 2	16539
Tspoap1	TSPO associated protein 1	207777
Cacna1d	calcium channel, voltage-dependent, L type, alpha 1D subunit	12289
Trpc7	transient receptor potential cation channel. subfamily C, member 7	26946
Abcc9	ATP-binding cassette, sub-family C (CFTR/MRP), member 9	20928
Scn4b	sodium channel, type IV, beta	399548
Htr3a	5-hydroxytryptamine (serotonin) receptor 3A	15561
Anxa2	annexin A2	12306
Itpr2	inositol 1,4,5-triphosphate receptor 2	16439
Trpc1	transient receptor potential cation channel. subfamily C. member 1	22063
Kcnmb4	potassium large conductance calcium-activated channel. subfamily M. beta member 4	58802
Cacng3	calcium channel, voltage-dependent, gamma subunit 3	54376
Cacng5	calcium channel, voltage-dependent, gamma subunit 5	140723
Tmem63c	transmembrane protein 63c	217733
Kcnip3	Kv channel interacting protein 3. calsenilin	56461
Kcnn4	potassium intermediate/small conductance calcium-activated channel, subfamily N, member 4	16534
Pex5l	peroxisomal biogenesis factor 5-like	58869
Panx1	pannexin 1	55991
Itpr1	inositol 1,4,5-trisphosphate receptor 1	16438
Kcnj14	potassium inwardly-rectifying channel, subfamily J, member 14	211480

Supplementary Table S3. GO term: Axoneme part. ID: 0044447; size=37; overlap=9; Enrichment Ratio=1.01; p=4.738e-7; FDR=3.433e-3

Gene Symbol	Gene Name	Entrez Gene
Dnah9	dynein, axonemal, heavy chain 9	237806
Cfap206	cilia and flagella associated protein 206	69329
Arfgef2	ADP-ribosylation factor guanine nucleotide-exchange factor 2 (brefeldin A-inhibited)	99371
Dnah5	dynein, axonemal, heavy chain 5	110082
Cfap100	cilia and flagella associated protein 100	243538
Rsph4a	radial spoke head 4 homolog A (Chlamydomonas)	212892
Dnah10	dynein, axonemal, heavy chain 10	56087
Dnah7a	dynein, axonemal, heavy chain 7A	627872
Cep162	centrosomal protein 162	382090

Supplementary Table S4. GO term: Cilium. ID: 0005929; size=559; overlap=37; Enrichment Ratio=2.43; p=5.834e-7; FDR=3.433e-3.

Gene Symbol	Gene Name	Entrez Gene
Iqcg	IQ motif containing G	69707
Mchr1	melanin-concentrating hormone receptor 1	207911
Mdm1	transformed mouse 3T3 cell double minute 1	17245
Ptpn23	protein tyrosine phosphatase. non-receptor type 23	104831
Smo	smoothened frizzled class receptor	319757
Intu	inturned planar cell polarity protein	380614
Dnah9	dynein axonemal heavy chain 9	237806
Cfap206	cilia and flagella associated protein 206	69329
Pdzd7	PDZ domain containing 7	100503041
Arfgef2	ADP-ribosylation factor guanine nucleotide-exchange factor 2 (brefeldin A-inhibited)	99371
Grk3	G protein-coupled receptor kinase 3	320129
1700012B09Rik	RIKEN cDNA 1700012B09 gene	69325
Dnah5	dynein axonemal heavy chain 5	110082
Kif3b	kinesin family member 3B	16569
Vipr2	vasoactive intestinal peptide receptor 2	22355
Oaz3	ornithine decarboxylase antizyme 3	53814
Efhc1	EF-hand domain (C-terminal) containing 1	71877
Aldoa	aldolase A. fructose-bisphosphate	11674
Iqce	IQ motif containing E	74239
Cfap100	cilia and flagella associated protein 100	243538
Myo3b	myosin IIIB	329421
Ezr	ezrin	22350
Rsph4a	radial spoke head 4 homolog A (Chlamydomonas)	212892
Sufu	SUFU negative regulator of hedgehog signaling	24069
Cfap52	cilia and flagella associated protein 52	71860
Dnah10	dynein axonemal heavy chain 10	56087
Armc4	armadillo repeat containing 4	74934
Dnah7a	dynein. axonemal. heavy chain 7A	627872
Nedd1	neural precursor cell expressed. developmentally down-regulated gene 1	17997

Cep162	centrosomal protein 162	382090
Calcr	calcitonin receptor	12311
Tekt1	tektin 1	21689
Shank2	SH3 and multiple ankyrin repeat domains 2	210274
Best2	bestrophin 2	212989
Prom2	prominin 2	192212
Cntrl	centriolin	26920
Spa17	sperm autoantigenic protein 17	20686

Supplementary Table S5. GO term: Metanephros development. ID: 0001656; size=84; overlap=11; Enrichment Ratio=2.28; p=1.651e-5; FDR=2.428e-2.

Gene Symbol	Gene Name	Entrez Gene
Wnt4	wingless-type MMTV integration site family. member 4	22417
Wwtr1	WW domain containing transcription regulator 1	97064
Calb1	calbindin 1	12307
Fras1	Fraser extracellular matrix complex subunit 1	231470
Fat4	FAT atypical cadherin 4	329628
Smo	smoothened. frizzled class receptor	319757
Irx2	Iroquois homeobox 2	16372
Aph1c	aph1 homolog C. gamma secretase subunit	68318
Eya1	EYA transcriptional coactivator and phosphatase 1	14048
Yap1	yes-associated protein 1	22601
Kif26b	kinesin family member 26B	269152

Supplementary Table S6. Opioid Reactome.

GENE SYMBOL	GENE NAME	ENTREZ GENE	LOG2(FC)	ES
Prkcg	protein kinase C gamma	5582	-0.431	0.002
Itpr1	inositol 1.4.5-trisphosphate receptor type 1	3708	-0.312	-0.08
Itpr2	inositol 1.4.5-trisphosphate receptor type 2	3709	-0.291	-0.042
Ppp1r1b	protein phosphatase 1 regulatory inhibitor subunit 1B	84152	-0.257	-0.106
Gnb3	G protein subunit beta 3	2784	-0.251	-0.2509
Nbea	neurobeachin	26960	-0.216	-0.134
Itpr3	inositol 1.4.5-trisphosphate receptor type 3	3710	-0.214	-0.2934
Adcy1	adenylate cyclase 1	107	-0.203	-0.231
Adcy6	adenylate cyclase 6	112	-0.198	-0.191
Creb1	cAMP responsive element binding protein 1	1385	-0.196	-0.1635
Prkcd	protein kinase C delta	5580	-0.184	-0.254
Gng5	G protein subunit gamma 5	2787	-0.184	-0.21
Adcy5	adenylate cyclase 5	111	-0.164	-0.276
Ppp3cc	protein phosphatase 3 catalytic subunit gamma	5533	-0.145	-0.2576
Gng8	G protein subunit gamma 8	94235	-0.141	-0.306
Gng12	G protein subunit gamma 12	55970	-0.121	-0.316
Gng11	G protein subunit gamma 11	2791	-0.116	-0.291
Gna15	G protein subunit alpha 15	2769	-0.114	-0.3073
Pde1C	phosphodiesterase 1C	5137	-0.112	-0.351
Camk2a	calcium/calmodulin dependent protein kinase II alpha	815	-0.112	-0.3324
Gna14	G protein subunit alpha 14	9630	-0.101	-0.347
Gngt2	G protein subunit gamma transducin 2	2793	-0.09	-0.358
Pde4c	phosphodiesterase 4C	5143	-0.088	-0.2774
Adcy9	adenylate cyclase 9	115	-0.083	-0.354
Plcb2	phospholipase C beta 2	5330	-0.069	-0.227
Ppp2r1b	protein phosphatase 2 scaffold subunit abeta	5519	-0.061	-0.28
Ppp1ca	protein phosphatase 1 catalytic subunit alpha	5499	-0.06	-0.3
Camk4	calcium/calmodulin dependent protein kinase IV	814	-0.045	-0.343

Camk2g	calcium/calmodulin dependent protein kinase II gamma	818	-0.036	-0.324
Pdyn	prodynorphin	5173	-0.027	-0.2838
Gng13	G protein subunit gamma 13	51764	-0.026	-0.261
Gna11	G protein subunit alpha 11	2767	-0.024	-0.2194
Gna1	G protein subunit alpha i1	2770	-0.024	-0.219
Ppp3ca	protein phosphatase 3 catalytic subunit alpha	5530	-0.015	-0.267
Gng10	G protein subunit gamma 10	2790	-0.015	-0.255
Kpna2	karyopherin subunit alpha 2	3838	-0.015	-0.187
Camk2d	calcium/calmodulin dependent protein kinase II delta	817	-0.012	-0.188
Camk2b	calcium/calmodulin dependent protein kinase II beta	816	-0.012	-0.1876
Adcy3	adenylate cyclase 3	109	-0.005	-0.149
Grk2	G protein-coupled receptor kinase 2	156	-0.005	-0.117
Adcy8	adenylate cyclase 8	114	-0.003	-0.109
Prkca	protein kinase C alpha	5578	-0.002	-0.202
Prkcg	protein kinase C gamma	5582	-0.431	0.002
Itpr1	inositol 1.4.5-trisphosphate receptor type 1	3708	-0.312	-0.08
Itpr2	inositol 1.4.5-trisphosphate receptor type 2	3709	-0.291	-0.042
Ppp1r1b	protein phosphatase 1 regulatory inhibitor subunit 1B	84152	-0.257	-0.106
Gnb3	G protein subunit beta 3	2784	-0.251	-0.2509
Nbea	neurobeachin	26960	-0.216	-0.134
Itpr3	inositol 1.4.5-trisphosphate receptor type 3	3710	-0.214	-0.2934
Adcy1	adenylate cyclase 1	107	-0.203	-0.231
Adcy6	adenylate cyclase 6	112	-0.198	-0.191
Creb1	cAMP responsive element binding protein 1	1385	-0.196	-0.1635
Prkcd	protein kinase C delta	5580	-0.184	-0.254
Gng5	G protein subunit gamma 5	2787	-0.184	-0.21
Adcy5	adenylate cyclase 5	111	-0.164	-0.276
Ppp3cc	protein phosphatase 3 catalytic subunit gamma	5533	-0.145	-0.2576
Gng8	G protein subunit gamma 8	94235	-0.141	-0.306
Gng12	G protein subunit gamma 12	55970	-0.121	-0.316
Gng11	G protein subunit gamma 11	2791	-0.116	-0.291

Gna15	G protein subunit alpha 15	2769	-0.114	-0.3073
Pde1C	phosphodiesterase 1C	5137	-0.112	-0.351
Camk2a	calcium/calmodulin dependent protein kinase II alpha	815	-0.112	-0.3324
Gna14	G protein subunit alpha 14	9630	-0.101	-0.347
Gngt2	G protein subunit gamma transducin 2	2793	-0.09	-0.358
Pde4c	phosphodiesterase 4C	5143	-0.088	-0.2774
Adcy9	adenylate cyclase 9	115	-0.083	-0.354
Plcb2	phospholipase C beta 2	5330	-0.069	-0.227
Ppp2r1b	protein phosphatase 2 scaffold subunit abeta	5519	-0.061	-0.28
Ppp1ca	protein phosphatase 1 catalytic subunit alpha	5499	-0.06	-0.3
Camk4	calcium/calmodulin dependent protein kinase IV	814	-0.045	-0.343
Camk2g	calcium/calmodulin dependent protein kinase II gamma	818	-0.036	-0.324
Pdyn	prodynorphin	5173	-0.027	-0.2838
Gng13	G protein subunit gamma 13	51764	-0.026	-0.261
Gna11	G protein subunit alpha 11	2767	-0.024	-0.2194
Gna1	G protein subunit alpha i1	2770	-0.024	-0.219
Ppp3ca	protein phosphatase 3 catalytic subunit alpha	5530	-0.015	-0.267
Gng10	G protein subunit gamma 10	2790	-0.015	-0.255
Kpna2	karyopherin subunit alpha 2	3838	-0.015	-0.187
Camk2d	calcium/calmodulin dependent protein kinase II delta	817	-0.012	-0.188
Camk2b	calcium/calmodulin dependent protein kinase II beta	816	-0.012	-0.1876
Adcy3	adenylate cyclase 3	109	-0.005	-0.149
Grk2	G protein-coupled receptor kinase 2	156	-0.005	-0.117
Adcy8	adenylate cyclase 8	114	-0.003	-0.109
Prkca	protein kinase C alpha	5578	-0.002	-0.202

Supplementary Table S7. Details of statistical analyses for main Figures 1-2.

Figure number	Test	Statistical analysis	Factor Name	Statistic Value	P-value
Fig 1B	TRAP - PCA - Factor 1	Two-way RM ANOVA	Fraction	F (1, 9) = 298.3	p<0.0001
			Treatment	F (1, 9) = 0.02524	p=0.8773
			Fraction x Treatment	F (1, 9) = 0.2735	p=0.6137
Fig 1C	Oprm1 counts	Two-way RM ANOVA	Fraction	F (1, 9) = 15.11	p=0.0037
			Treatment	F (1, 9) = 0.4898	p=0.5017
			Fraction x Treatment	F (1, 9) = 0.04840	p=0.8308
Fig 1D	mCherry counts	Two-way RM ANOVA	Fraction	F (1, 9) = 6.994	p=0.0267
			Treatment	F (1, 9) = 0.2792	p=0.6100
			Fraction x Treatment	F (1, 9) = 0.3184	p=0.5864
Fig 2B	Log2(FC) of DE genes in input and IP	One sample t-test; theoretical mean: 0	Input	t=2.908, df=616	p=0.0038
		One sample t-test; theoretical mean: 0	IP	t=9.884, df=612	p<0.0001
		two-tailed unpaired t-test with Welch's correction	Fraction effect	t=5.755, df=1186	p<0.0001
Fig 2C	Log2(FC) of genes IP vs Input	two-tailed unpaired t-test with Welch's correction	DE after morphine	t=7.966, df=621.5	p<0.0001
Fig 2D	ORA GO terms	FDR BH	/	/	see legends
Fig 2E	GSEA IP ABS vs CTL	FDR BH	/	q=0.04189189	
Fig 2F	GSEA IP vs input	FDR BH	/	IP vs input CTL. q=0.18007663 IP vs input ABS. q=0.35191083	

Supplementary Table S8. Details of statistical analyses for main Figure 3

Figure number	Test	Statistical analysis	Factor Name	Statistic Value	P-value
Fig 3B	oICSSS acquisition - nosepoke	Three-way RM ANOVA	Sessions	F (27, 864) = 23.52	P<0.0001
			Nosepoke	F (1, 32) = 279.3	P<0.0001
			Treatment	F (1, 32) = 1.917	P=0.1758
			Sessions x Nosepoke	F (27, 864) = 36.91	P<0.0001
			Sessions x Treatment	F (27, 864) = 0.4305	P=0.9953
			Nosepoke x Treatment	F (1, 32) = 2.166	P=0.1509
			Sessions x Nosepoke x Treatment	F (27, 864) = 0.4365	P=0.9948
Fig 3B'	oICSSS acquisition - Mean nosepoke	Three-way RM ANOVA	Schedule	F (2, 64) = 52.52	P<0.0001
			Nosepoke	F (1, 32) = 283.3	P<0.0001
			Treatment	F (1, 32) = 2.123	P=0.1548
			Schedule x Nosepoke	F (2, 64) = 93.47	P<0.0001
			Schedule x Treatment	F (2, 64) = 0.1446	P=0.8657
			Nosepoke x Treatment	F (1, 32) = 2.609	P=0.1161
			Schedule x Nosepoke x Treatment	F (2, 64) = 0.2336	P=0.7923
Fig 3C	Laser Stimulation	Two-way RM ANOVA	Sessions	F (4.448, 142.3) = 7.261	P<0.0001
			Treatment	F (1, 32) = 1.271	P=0.2679
			Sessions x Treatment	F (27, 864) = 0.4221	P=0.9960
Fig 3C'	Mean laser Stimulation	Two-way RM ANOVA	Schedule	F (1.654, 52.92) = 2.444	P=0.1059
			Treatment	F (1, 32) = 1.128	P=0.2962
			Schedule x Treatment	F (2, 64) = 0.03918	P=0.9616

Supplementary Table S9. Details of statistical analyses for main Figure 4.

Figure number	Test	Statistical analysis	Factor Name	Statistic Value	P-value
Fig 4A	Impulsivity-like nosepokes	Three-way RM ANOVA	Sessions	F (27, 864) = 8.679	P<0.0001
			Nosepoke	F (1, 32) = 68.37	P<0.0001
			Treatment	F (1, 32) = 6.253	P=0.0177
			Sessions x Nosepoke	F (27, 864) = 8.646	P<0.0001
			Sessions x Treatment	F (27, 864) = 0.9952	P=0.4724
			Nosepoke x Treatment	F (1, 32) = 6.239	P=0.0178
			Sessions x Nosepoke x Treatment	F (27, 864) = 1.000	P=0.4655
Fig 4A'	Mean impulsivity-like nosepokes	Three-way RM ANOVA	Schedule	F (2, 64) = 16.86	P<0.0001
			Nosepoke	F (1, 32) = 53.67	P<0.0001
			Treatment	F (1, 32) = 4.571	P=0.0403
			Schedule x Nosepoke	F (2, 64) = 16.79	P<0.0001
			Schedule x Treatment	F (2, 64) = 1.039	P=0.3598
			Nosepoke x Treatment	F (1, 32) = 4.542	P=0.0409
			Schedule x Nosepoke x Treatment	F (2, 64) = 1.030	P=0.3630
Fig 4B	Persistence to response FR3	three-way RM ANOVA	Sessions	F (3, 96) = 1.905	P=0.1340
			Nosepoke	F (1, 32) = 196.6	P<0.0001
			Treatment	F (1, 32) = 5.572	P=0.0245
			Sessions x Nosepoke	F (3, 96) = 2.318	P=0.0803
			Sessions x Treatment	F (3, 96) = 1.420	P=0.2417
			Nosepoke x Treatment	F (1, 32) = 6.404	P=0.0165
			Sessions x Nosepoke x Treatment	F (3, 96) = 2.270	P=0.0853
Fig 4B'	Persistence to response FR5	three-way RM ANOVA	Sessions	F (3, 96) = 0.9947	P=0.3988
			Nosepoke	F (1, 32) = 87.93	P<0.0001
			Treatment	F (1, 32) = 8.426e-006	P=0.9977
			Sessions x Nosepoke	F (3, 96) = 0.7337	P=0.5344
			Sessions x Treatment	F (3, 96) = 0.6654	P=0.5753
			Nosepoke x Treatment	F (1, 32) = 0.004364	P=0.9477

			Sessions x Nosepoke x Treatment	F (3, 96) = 0.6784	P=0.5674
Fig 4D	Motivation	unpaired t-test	Treatment	t=0.549, df=31	p=0.5865
Fig 4C	Compulsivity	unpaired t-test	Treatment	t=1.815, df=30	p=0.0796
Fig 4E	Extinction and Reinstatement	two-way RM ANOVA	Cue	F (1, 30) = 8.000	P=0.0083
			Treatment	F (1, 30) = 0.8903	P=0.3529
			Cue x Treatment	F (1, 30) = 0.001602	P=0.9683

Supplementary Table S10. Details of statistical analyses for main Figure 5.

Figure number	Test	Statistical analysis	Factor Name	Statistic Value	P-value
Fig 5A	3 crit / Persistence to respond	Kruskal-wallis test	Criteria	Kruskal-wallis statistic: 18.59	p=0.0003
Fig 5B	3 crit / Motivation	Kruskal-wallis test	Criteria	Kruskal-wallis statistic: 13.42	P=0.0038
Fig 5C	3 crit / Compulsivity	Kruskal-wallis test	Criteria	Kruskal-wallis statistic: 8.693	P=0.0337
Fig 5E	3 crit / average	Chi-square test for trend	Treatment	t=5.846. df=1	p=0.0156
Fig 5G	PCA	One-way ANOVA - 3crit	Factor 1	F(3, 30)=25.68	p<0.0001
			Factor 2	F(3, 30)=1.108	p=0.36
Fig 5H	PCA	unpaired t-test - Treatment	Factor 1	t=-2.17. df=31	p=0.037
			Factor 2	t=0.417. df=31	p=0.68

Supplementary Table S11. Details of statistical analyses for supplementary figures.

Figure number	Test	Statistical analysis	Factor Name	Statistic Value	P-value
S1	Millions of read	Two-way ANOVA	Fraction	F (1, 18) = 1.344	p=0.2616
			Treatment	F (1, 18) = 0.09282	p=0.7641
			Fraction x Treatment	F (1, 18) = 0.1901	p=0.6680
S2	GSEA - IP vs input CTL - scRNA-seq	FDR BH procedure	/	5HT-II: q=0.00089; Glu-IV: q=0.00045; Glu-III: q=0.0005; Poly2: q=0.00058; GABA-II: q=0.00162; Glu-I: q=0.00178; GABA-I: q=0.00223	
S4A	mCh - oICSS acquisiton	two-way RM ANOVA	Sessions	F (27, 81) = 1.665	p=0.0418
			Nosepoke	F (1, 3) = 3.595	p=0.1542
			Sessions x Nosepoke	F (27, 81) = 1.381	p=0.1353
S4B	cFos expression	Kruskal-Wallis test	Virus	Kruskal-Wallis Statistic : 8.715	p=0.0055
S5B	Nosepoke during LS	Two-way RM ANOVA	Sessions	F (27, 862) = 5.543	p<0.0001
			Treatment	F (1, 32) = 0.1501	p=0.7010
			Session x Treatment	F (27, 862) = 0.1186	p>0.9999
S5C	Number of back and forths	Two-way RM ANOVA	Sessions	F (27, 864) = 11.85	p<0.0001
			Treatment	F (1, 32) = 0.6669	p=0.4202
			Session x Treatment	F (27, 864) = 1.017	p=0.4415
S6A	Effect of FS on nosepoke	Two-way RM ANOVA	Sessions	F (6, 192) = 25.34	p<0.0001
			Treatment	F (1, 32) = 0.7848	p=0.3823
			Session x Treatment	F (6, 192) = 0.3187	p=0.9267
S6B	Effect of FS on LS	Two-way RM ANOVA	Sessions	F (6, 198) = 35.21	p<0.0001
			Treatment	F (1, 32) = 0.6622	p=0.4218
			Session x Treatment	F (32, 198) = 10.83	p<0.0001

REFERENCES

1. Goeldner, C., et al., *Impaired emotional-like behavior and serotonergic function during protracted abstinence from chronic morphine.* Biological psychiatry, 2011. **69**(3): p. 236-244.
2. Nectow, A.R., et al., *Rapid Molecular Profiling of Defined Cell Types Using Viral TRAP.* Cell Rep, 2017. **19**(3): p. 655-667.
3. Heiman, M., et al., *A Translational Profiling Approach for the Molecular Characterization of CNS Cell Types.* Cell, 2008. **135**(4): p. 738-748.
4. Heiman, M., et al., *Cell type-specific mRNA purification by translating ribosome affinity purification (TRAP).* Nat Protoc, 2014. **9**(6): p. 1282-91.
5. Love, M.I., W. Huber, and S. Anders, *Moderated estimation of fold change and dispersion for RNA-seq data with DESeq2.* Genome Biology, 2014. **15**(12): p. 550.
6. Liao, Y., et al., *WebGestalt 2019: gene set analysis toolkit with revamped UIs and APIs.* Nucleic Acids Res, 2019. **47**(W1): p. W199-w205.
7. Subramanian, A., et al., *Gene set enrichment analysis: A knowledge-based approach for interpreting genome-wide expression profiles.* Proceedings of the National Academy of Sciences, 2005. **102**(43): p. 15545-15550.
8. Huang, K.W., et al., *Molecular and anatomical organization of the dorsal raphe nucleus.* eLife, 2019. **8**: p. e46464.
9. Jassal, B.L.N., N., *Opioid Signalling.* Reactome, 2004.
10. Pascoli, V., et al., *Sufficiency of Mesolimbic Dopamine Neuron Stimulation for the Progression to Addiction.* Neuron, 2015. **88**(5): p. 1054-1066.
11. Martín-García, E., et al., *New operant model of reinstatement of food-seeking behavior in mice.* Psychopharmacology, 2011. **215**(1): p. 49-70.
12. Domingo-Rodriguez, L., et al., *A specific prelimbic-nucleus accumbens pathway controls resilience versus vulnerability to food addiction.* Nature Communications, 2020. **11**(1): p. 782.
13. Richardson, N.R. and D.C. Roberts, *Progressive ratio schedules in drug self-administration studies in rats: a method to evaluate reinforcing efficacy.* J Neurosci Methods, 1996. **66**(1): p. 1-11.
14. Vollmer, K.M., et al., *A Novel Assay Allowing Drug Self-Administration, Extinction, and Reinstatement Testing in Head-Restrained Mice.* Frontiers in Behavioral Neuroscience, 2021. **15**.
15. Deroche-Gamonet, V., D. Belin, and P.V. Piazza, *Evidence for Addiction-like Behavior in the Rat.* Science, 2004. **305**(5686): p. 1014-1017.